J. Fluid Mech. (1995), *vol.* 285, *pp.* 215–247

Streamline topology in eccentric Taylor vortex flow†

By P. ASHWIN[1] AND G. P. KING[1,2]

[1] Mathematics Institute, University of Warwick, Coventry CV4 7AL, UK

[2] Department of Engineering, University of Warwick, Coventry CV4 7AL, UK

(Received 26 November 1993 and in revised form 21 September 1994)

We investigate an asymptotic model of DiPrima & Stuart (1972*b*, 1975) describing steady Taylor vortex flow between eccentric cylinders, under the assumption that the eccentricity ϵ, the clearance ratio δ and the Taylor vortex amplitude A satisfy ϵ, δ and A small. By solving a boundary value problem for the radial eigenfunctions we numerically obtain the flow field of DiPrima & Stuart and investigate its topology, after correcting higher-order terms to ensure that the flow preserves volume. We find regions of chaotic streamlines at all eccentricities and discuss the reason for their existence. We make an analogy between the full model and a modulated vortex flow field which qualitatively displays the same behaviour.

For large eccentricities, we examine the flow field and the topology of its streamlines, especially where the two-dimensional flow contains a separated region of recirculation. In this case Taylor vortices give rise to transport of fluid particles in and out of the separated region. We find that the onset of Taylor vortices encourages recirculation in the inflow plane, whilst discouraging it in the outflow plane.

1. Introduction

In the 1960s Arnol'd (1965) and Hénon (1965) used dynamical systems theory to argue that a steady three-dimensional flow may give rise to chaotic streamlines. At present there exist few studies of chaotic streamlines in steady three-dimensional flows: Beltrami flow solutions of the Euler equation (e.g. ABC flows (Hénon 1965; Dombre *et al.* 1986); thermal convection in a periodic box (Arter 1983); twisted pipe flow (Jones, Thomas & Aref 1989); flow in a heat exchanger (Acharya, Sen & Chang 1993)). The lack of examples is easily understood: it is very difficult to derive three-dimensional solutions to the equations of fluid motion without using some continuous symmetry to reduce the dimensionality of the problem. For this reason, most attention has been focused on chaotic particle paths (i.e. chaotic advection) in unsteady two-dimensional flows (cf. Aref 1984 and the special issue *Physics of Fluids* A 3, 1991).

One fully three-dimensional, steady flow solution was derived some time ago by DiPrima & Stuart (1972*a*, *b*, 1975) for Taylor vortex flow between eccentric rotating cylinders for the case of small eccentricity, small gap and Taylor numbers slightly greater than critical. We have investigated their solution for the case of a rotating inner cylinder and a stationary outer cylinder and describe in this paper the streamline topology and chaotic advection that it gives rise to.

The classical Taylor–Couette problem consists of infinitely long concentric cylinders and an incompressible Newtonian fluid between them. On rotating the inner cylinder

† With Appendix B by G. Rowlands.

at a constant angular velocity, the fluid is forced into motion by the non-slip condition on the walls of the container. For values of the Taylor number T (which gives a non-dimensional rate of rotation) less than a critical value T_c, the only stable flow field is circular Couette flow, a two-dimensional flow in planes perpendicular to the axis of the cylinders, where all streamlines are closed circles. Increasing T past T_c gives rise to steady Taylor vortices, ideally through a pitchfork bifurcation. Although the flow is now three-dimensional, the rotational symmetry constrains the streamlines to lie on the surface of stream tubes (tori) nested within each other.

The rotational symmetry reduces the problem to two dimensions and hence it must be broken in order to obtain a fully three-dimensional steady flow. This is easily done by displacing one of the cylinders to an eccentric position, a geometry of interest in lubrication technology as well as hydrodynamic stability theory.

The motivation for this paper came from the desire to apply dynamical systems thinking to guess the effect of eccentricity on the streamlines of Taylor vortices. This led to the following two 'generic' predictions.

First, small eccentricity results in a perturbed system which should show similarity to an area-preserving twist map perturbed from integrability. This should give rise to the presence of KAM surfaces separating chaotic regions (cf. Ottino 1989), and the measure of the chaotic regions should tend to zero as the eccentricity tends to zero.

Our second prediction concerns what should happen at large eccentricity. From studies of the basic two-dimensional flow it is well known that at sufficiently large eccentricity an eddy in the region of widest gap is created by the separation of the fluid from the outer boundary and its reattachment downstream (cf. Ballal & Rivlin 1977). The flow is divided by an invariant surface known as the 'dividing streamline' which connects the points of separation and reattachment as figure 2(*c*) illustrates. The region of recirculating separated flow persists after the formation of Taylor vortices (cf. Koschmieder 1976), but is now three-dimensional. Naively one might think that the dividing streamline has become a dividing streamsurface, thus forming a separated vortex whose streamlines never cross the dividing streamsurface. However, dynamical systems theory predicts a more complicated streamline topology: the separation surface emanating from the line of separation (the line connecting the points of separation in the inflow and outflow boundaries) and the surface of reattachment emanating from the line of reattachment will not usually coincide. Instead these surfaces will intersect transversely in one-dimensional sets an infinite number of times. Thus a separated vortex will not occur and streamlines will wander chaotically in and out of the region of recirculation (looking ahead to figure 9).

The model we investigate is an asymptotic approximation of an exact solution to the Navier–Stokes equations. We must be concerned therefore with whether or not the approximate solution, at a given truncation of the expansion, models the physically important processes sufficiently well to have confidence in its predictions. It is certainly true that the approximate solution only approximately satisfies conservation of volume (i.e. $\nabla \cdot \boldsymbol{u}$ is only approximately zero – this is addressed in §4). There may be other constraints which are not satisfied, for example some sort of hidden conserved quantity which prevents chaotic mixing in all steady flows with these boundary conditions.† We have no reason to believe that there may be hidden constraints which the asymptotic solutions fails to retain, but we have to take this as a hypothesis to justify talking about generic volume-preserving flows. In order to assess the question of how well the

† Such a situation happens in steady Euler flows where it is necessary that the Beltrami condition is satisfied ($\boldsymbol{u} \cdot \nabla \times \boldsymbol{u} = 0$) in order to have the possibility of chaotic mixing.

asymptotic solution models the important physical processes, we have included a review of relevant experimental and numerical work. We have also studied the effect of changing the order of truncation of the equations from first to second. This results in only small quantitative changes to the streamline topology, even when there are large regions of chaotic mixing.

The paper is organized as follows. In §2 we describe the eccentric cylinder system and give a review of previous research into steady flows in such a geometry. Then in §3 we collect the necessary details from the papers of DiPrima & Stuart for flows with eccentricity, gap and Taylor vortex amplitude small. Their model is not immediately amenable to particle tracking investigations because it only approximately satisfies conservation of volume. In order to overcome this, we propose a modification to a simplified version of their model that ensures volume conservation by addition of higher-order terms. This is outlined in §4. Using this modified velocity field, results of some numerical investigations into the structure and mixing of this flow field are presented in §5. Streamlines (which are equivalent to particle paths in steady flows) are followed at a variety of parameter values and we observe the appearance of regions of chaotic mixing, even for small eccentricities. Pushing the model to large eccentricities, as noted by DiPrima & Stuart, there is prediction of a recirculation region in the largest gap. With the addition of Taylor vortex type perturbations, we observe the motion of fluid in and out of this recirculating region. In §6 we discuss our results and introduce a modulated vortex model to help understand the physics controlling the onset of chaotic advection in the small eccentricity limit. Using an analogy from plasma physics, G. Rowlands presents in Appendix B a derivation of a Poincaré map for this model in the small eccentricity limit. Finally, in §7 we point out what we feel are some interesting future directions of study.

2. The eccentric cylinder system

Figure 1 shows an eccentric cylinder system with inner and outer cylinders of radii a and b, and linear speeds $q_1 = a\Omega_1$ and $q_2 = b\Omega_2$ measured in the counter-clockwise direction. The centres of the cylinders are set a distance ae apart, where

$$e = \epsilon\delta, \quad \delta = d/a, \quad d = b-a, \tag{2.1}$$

$$\mu = \Omega_2/\Omega_1, \tag{2.2}$$

and

$$0 \leqslant \epsilon < 1. \tag{2.3}$$

In lubrication theory, ϵ is known as the eccentricity and δ as the clearance ratio. The radius ratio and clearance ratios are related by

$$\delta = \frac{1-\eta}{\eta}, \quad \eta = \frac{a}{b}. \tag{2.4}$$

In this paper we confine our attention to the case $\mu = 0$ (i.e. $q_2 = 0$). The conventional Reynolds and Taylor numbers are defined by

$$R = \frac{a\Omega_1 d}{\nu}, \tag{2.5}$$

$$T = \frac{a\Omega_1^2 d^3}{\nu^2}, \tag{2.6}$$

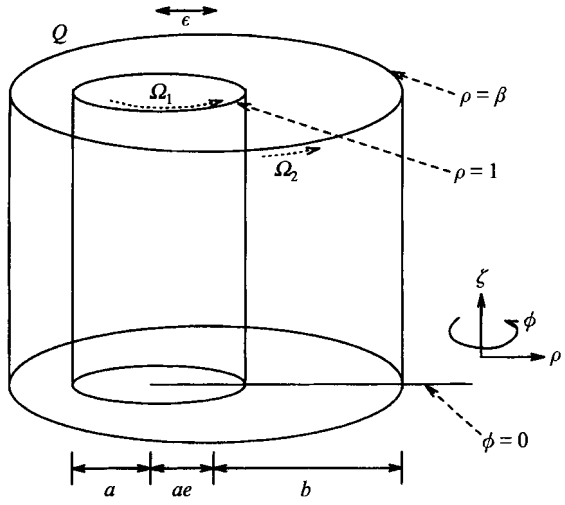

FIGURE 1. The geometry of the problem with the modified bipolar coordinates (ρ, ϕ, ζ) marked. The inner and outer cylinders (of radii a and b respectively) are rotated at frequencies Ω_1 and Ω_2 respectively. In our investigation, we take $a\Omega_1 = Q$ and $\Omega_2 = 0$.

and thus
$$R = \left(\frac{T}{\delta}\right)^{1/2}, \tag{2.7}$$

where ν is the kinematic viscosity.

We adopt the same notation used by DiPrima & Stuart in their papers. In particular, λ denotes the axial wavenumber.

2.1. *Phenomenology*

2.1.1. *The basic flow*

Sketches of streamlines of the Stokes flow when $q_2 = 0$ (q_1 asymptotically small) for $\epsilon = 0$, 0.2 and 0.5 are shown in figure 2. All streamlines except the dividing one in (*c*) are closed. When the cylinders are concentric, the basic flow is circular Couette flow and the streamlines are circles. When the cylinders are made non-concentric, the rotation of the inner cylinder gives rise to a varying, circumferential pressure gradient which results in a combined Couette and pressure flow around the cylinders. This is not axisymmetric. When ϵ is sufficiently large, the flow separates from the outer cylinder. The points of separation and reattachment are joined by the dividing streamline which separates the flow into two non-communicating regions. (See Ballal & Rivlin 1977 for a detailed analysis of the Stokes flow between eccentric cylinders.)

2.1.2. *Onset of Taylor vortices*

Linear stability analysis for concentric cylinders yields a Taylor number versus axial wavenumber marginal stability curve for the onset of Taylor vortices. The minimum of this stability curve yields T_c and λ_c. Steady Taylor vortices also arise as the primary instability for eccentric cylinders (at least for ϵ not too large). The dependence of T_c on ϵ has been studied experimentally by several authors (see Eagles, Stuart & DiPrima 1978 and references therein). These studies indicate that eccentricity is stabilizing when $\mu = 0$, but when $\mu > 0$ there is a range of ϵ where eccentricity can be destabilizing (see Versteegen & Jankowski 1969; Oikawa, Karasudani & Funakoshi 1989*a*; Raffaï & Laure 1991). The dependence of λ_c on ϵ has been studied experimentally for $\delta = 0.375$

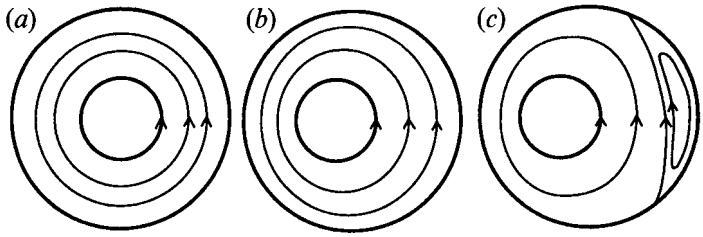

FIGURE 2. A sketch of the streamlines of basic two-dimensional Stokes flow for the case $\delta = 1$. We take $\Omega_2 = 0$ with (*a*) $\epsilon = 0$, (*b*) $\epsilon = 0.2$ and (*c*) $\epsilon = 0.5$. Note the region of recirculating fluid in (*c*). The effect of the inertial terms on the two-dimensional flow is to deform the flow and to give instability in the third direction via the Taylor vortex instability.

by Koschmieder (1976) and for $\delta = 0.205$ by Karasudani (1987), and numerically for $\delta = 0.1$, 0.205 and 1.0 (Oikawa *et al.* 1989*a*, *b*). For small gaps (i.e. $\delta < 0.375$) λ_c was found to remain nearly constant up to $\epsilon \approx 0.4$ and then increase rapidly with ϵ. In the large gap case ($\delta = 1.0$) λ_c increases rapidly with ϵ.

An explanation for the rapid increase in λ_c with ϵ for $\epsilon > 0.4$ was offered by Karasudani (1987). He noted that the rapid increase in λ_c began at values of ϵ close to the onset of separation in the basic two-dimensional flow. He argued that the streamline connecting the separation and reattachment points acted as a fluid boundary. The flow problem defined by this geometry is in some sense close to a concentric problem with a smaller gap. Thus one expects both an increase in the critical Taylor number as well as an increase in λ_c.

Experiments by Vohr (1968) ($\delta = 0.099$, $\epsilon > 0.707$) and Karasudani (1987) ($\delta = 0.205$, $\epsilon > 0.6$) show that when ϵ becomes too large, no steady vortex flows are found. It is interesting to note that in their numerical linear stability analysis for $\delta = 0.1$, Oikawa *et al.* (1989*b*) found that the least stable eigenvalues are real for all cases calculated except for $\epsilon = 0.7$.

2.1.3. *Position of maximum vortex activity*

According to the DiPrima (1963) local stability theory, based on the parallel flow assumption, the most unstable position is the position of widest gap $\Theta = 0$ (Θ is the polar angle measured around the outside cylinder). DiPrima & Stuart (1972*b*) defined the vortex activity as the radial gradient of the axial velocity at the outer cylinder and obtained, by successive improvements in their analysis, $\Theta_m = 90°$, then $\Theta_m = 76°$ in DiPrima & Stuart (1975), and $\Theta_m = 49°$ in Eagles *et al.* (1978). It should be kept in mind that these values are obtained for $\lambda = 3.127$.

In his experiments, Vohr observed that the apparent intensity of vortex circulation varied considerably around eccentric cylinders. He remarked that at $\epsilon = 0.475$ the vortices were observed to be most strongly developed at a point approximately 50° downstream of the point of widest gap at $T = 1.2T_c$. (T_c is the critical Taylor number for the onset of Taylor vortices at $\epsilon = 0.475$. Note that throughout this paper T_c refers to the critical Taylor number at the relevant δ, ϵ and λ.)

In a wider gap system ($\delta = 0.375$), Koschmieder reported being unable to locate a position of maximum vortex activity by visual observation. His results suggest that the variation in vortex activity around the cylinder becomes weaker as δ increases.

Oikawa *et al.* (1989*b*) computed steady Taylor vortex flows at several Reynolds numbers for (δ, ϵ) = (0.1, 0.475) and (0.205, 0.5). For the case (δ, ϵ) = (0.1, 0.475), computed with λ set to 3.273, they found $\Theta_m = 97.8°$, 85°, 100.7° at $T/T_c = 1.08$, 1.19, 1.31 respectively. The result $\Theta_m = 85°$ at $T = 1.19T_c$ corresponds to Vohr's conditions.

Oikawa *et al.* point out that at these parameter values the radial gradient of the axial velocity exhibits an exceptionally wide, flat peak, and note that in such a case it would be difficult to determine Θ_m accurately by flow visualization. For the case $(\delta, \epsilon) = (0.205, 0.5)$, computed for $\lambda = 3.345$, they found that Θ_m decreased from 115.9° at $T = 1.02T_c$ to 101.6° at $T = 1.17T_c$, and then increased again to 113.3° at $T = 1.75T_c$.

On the other hand, Dai, Dong & Szeri (1992) computed Taylor vortex flows for a system with $(\delta, \epsilon) = (0.096, 0.4)$ with $\lambda = 3.127$ and found that Θ_m decreased monotonically from 90° at $T = T_c$ to about 58° at $T = 1.3T_c$. At $T \approx 1.2T_c$ they obtain $\Theta_m \approx 63°$. Their results clearly show a different trend for the dependence of Θ_m on T, but they did not study its dependence on ϵ.

In summary, the situation is this:

(i) The DiPrima & Stuart model predicts that when λ is set to 3.127, the position of maximum vortex activity decreases monotonically from 90° at $T = T_c$ to 49° at $T = 1.2T_c$. They do not discuss the general dependence of Θ_m on T, δ, ϵ, though this may be recovered from their papers.

(ii) Dai *et al.* find that for a smaller eccentricity ($\epsilon = 0.4$) but the same λ used by DiPrima & Stuart, Θ_m decreases monotonically from 90° at $T = T_c$ to about 63° at $T = 1.2T_c$, which is in agreement with the trend predicted by the DiPrima & Stuart model.

(iii) Oikawa *et al.* computations use (apart from λ) the same parameter values as Eagles *et al.* They find that for $T \geqslant T_c$, Θ_m is larger than 90° and oscillates in value as T is increased to $1.19T_c$. They find a similar situation for a larger gap system ($\delta = 0.205$).

It is tempting to conclude that Oikawa *et al.*'s results show that Vohr's conditions lie well outside the domain of validity of the asymptotic model. However, it should be noted that there is at present insufficient numerical and experimental data available to state how Θ_m varies with the parameters T, δ, ϵ and λ. In particular, it should be borne in mind that the dependence of Θ_m on λ has yet to be investigated. Although the value used by Oikawa *et al.* ($\lambda = 3.273$) is only 5% larger than that used by Eagles *et al.* and Dai *et al.*, it may prove significant. Because Vohr's observation was subjective and qualitative it cannot be used to clarify the situation. Clearly further work is required.

2.1.4. *Taylor vortices and separated flow*

A region of reversed flow, which makes its first appearance in the basic two-dimensional flow, also occurs in the region of widest gap after onset of Taylor vortices (Vohr 1968; Koschmieder 1976; DiPrima & Stuart 1972*a*; O'Brien, Jones & Mobbs 1974; Dai *et al.* 1992).

The variation in the angular position of the separation and reattachment points with eccentricity after the onset of Taylor vortices was investigated by O'Brien *et al.* (1974) in an apparatus with $\delta = 0.1$. They reported that near T_c the positions of the separation points are not axially dependent and do not depart greatly from the positions observed at T_c. However, as T is increased, the positions of the separation points become axially dependent. They also report that separation at the outer cylinder wall is delayed in the vicinity of the outflow boundary between vortex pairs. Inspection of their figure 2 shows that the positions of separation and reattachment are asymmetric about the position of widest gap. As ϵ is increased, both points move in the direction of rotation of the inner cylinder.

According to the DiPrima & Stuart (1972*a*) perturbation theory for the basic flow, separation is expected to occur at $\epsilon > 0.317$ for $\delta = 0.375$. In agreement with this prediction Koschmieder (1976) observed separation at T_c for $\epsilon = 0.371$ but not for

$\epsilon = 0.278$. Surprisingly however, separation was observed at $\epsilon = 0.278$ when $T > T_c$. Koschmieder also observed that as T was increased the separation line moved upstream at both eccentricities.

Recently Dai *et al.* (1992) computed Taylor vortex flows for a system $\delta = 0.096$, and studied the qualitative changes to the flow pattern as T increases past T_c for $\epsilon > 0.3$. They found that for $\epsilon = 0.4$ and $T < T_c$, the flow is two-dimensional and contains a region of recirculation. When T is increased past T_c, Taylor vortices develop, distorting the recirculation pattern. On increasing T further, the axial dimension of the domain that contains the recirculation gradually shrinks while its radial dimension at the position of widest gap increases in the in-going jet and decreases in the out-going jet between vortices. By $T \approx 1.4T_c$ the recirculation pattern has disappeared in the outward jet, and the axial dimension of the domain has decreased to about half the vertical dimension of a vortex. They also find that the recirculation domain is not symmetric with respect to the angular position of the widest gap. They describe the recirculation region as being 'bounded by a closed surface of vanishing radial velocity...'. Comparison of their figures 6*d* and 7 suggests that they identified instead a surface corresponding to vanishing tangential velocity. (This has been confirmed by Professor Szeri.)

Summarizing, it has been found that Taylor vortices have the following effect on separated flow:

(i) The outflow jet suppresses and the inflow jet enhances the recirculation region.

(ii) As $T - T_c$ is increased, the domain of recirculation deforms and shrinks in the axial direction, eventually disappearing in the outflow.

(iii) Flow separation occurs for values of ϵ less than that for the basic flow.

3. The DiPrima & Stuart model

From here on we will refer to DiPrima & Stuart (1972*a*) as paper I, DiPrima & Stuart (1972*b*) as paper II and Eagles *et al.* (1978) as paper III, indicating which equations we are using (as in Eagles *et al.* 1978).

3.1 *The stability problem*

The stability problem was first considered by DiPrima (1963) who developed a local theory based on the parallel flow assumption, commonly used in boundary-layer stability, viz. the effect of azimuthal dependence of the tangential velocity is neglected. This theory gives a 'local' criterion for instability, local in the sense of having a critical Taylor number, T_c, for each angle around the cylinder. Specifically, the local theory predicted the flow to be least stable at the position of widest gap.

An explanation of Vohr's observation of a position of maximum vortex activity 50° downstream from the position of widest gap was achieved by the 'global' theory of paper II which takes into account the fact that the basic flow depends on two coordinates (radial and azimuthal). This feature results in stability equations that are partial differential equations. The solution required is a 'global' one, in that the flow field at all points must affect the stability characteristics. Additional goals of the theory were to predict how the critical Taylor number for the onset of Taylor vortices, T_c, varied with ϵ, and to determine how the torque and load on the cylinders were affected by eccentricity. We now follow paper III closely and summarize the results of papers I, II and III.

In paper I, DiPrima & Stuart derived the flow field between eccentric cylinders from the Navier–Stokes equations by an expansion in two small parameters, δ and R_m,

where R_m is a modified Reynolds number proportional to $q_1(b-a)^2/a\nu$, and ϵ was followed to take any value in the range $0 \leqslant \epsilon < 1$. Their perturbation theory predicted separation of the basic flow when

$$\epsilon > 0.3028 + 0.0382\delta. \tag{3.1}$$

In paper II, DiPrima & Stuart pointed out that their approximation to the tangential velocity of the basic flow V (II, 4.11) preserves the property of two-dimensional flow separation for $\epsilon \geqslant 0.28$ (see II, p. 402, below (II, 4.18)), a result which is different from their two-dimensional result of I quoted in (II, 2.17) and shown here as equation (3.1). The linear stability of the basic flow was considered through a calculation to order ϵ^2 in which $\delta^{1/2}$ was held proportional to ϵ as this tended to zero. The resulting T_c (for $\lambda_c = 3.127$) is given in equation (III, 4.3):

$$T_c = 1694.97(1+1.1618\delta)(1+2.6185\epsilon^2) + O(\delta^2, \epsilon^2\delta, \epsilon^4). \tag{3.2}$$

The dependence on ϵ and δ gave slow increase with ϵ, in close agreement to many observations (see figures 2, 3 and 4 of paper III). An additional prediction was that, since the stability problem is non-local, the position of maximum vortex activity lies not at the position of maximum gap, where the basic flow is most unstable, but is shifted substantially downstream, in qualitative agreement with Vohr's observation. The angular position given by this theory is 90°.

In paper III, the perturbation equations were nonlinear in the Taylor vortex amplitude, but the expansion was taken only to order ϵ. Nonlinear and eccentric effects were brought in simultaneously by making the Taylor vortex amplitude proportional to $\epsilon^{1/2}$. An improved prediction of 76° was obtained for the position of maximum vortex activity.

Finally in paper III, the nonlinear calculation was taken to higher order and a prediction of 49° for the angular position of the position of maximum vortex activity was obtained. Such excellent agreement with Vohr's observation is unexpected (as III, p. 222 made clear) since the 'small' parameters are outside the range for which perturbation theory is expected to be valid. As mentioned before, the dependence of maximum vortex activity on T and ϵ requires further study.

3.2. *The coordinate system*

We assume no-slip boundary conditions at the cylinder walls, and periodic boundary conditions in the ζ-direction. We consider the flow field when the outer cylinder is stationary and the inner cylinder is rotated about its axis at a uniform linear velocity Q. This assumption means that in the notation of DiPrima & Stuart (1975) we set

$$q_1 = Q, \quad q_2 = 0,$$

implying that $c = 2(q_1-q_2)/(q_1+q_2) = 2$ in I, II and III. Naturally, it is possible to perform similar numerical experiments for more general values of q_1 and q_2.

We first introduce the modified bipolar coordinate system of Wood (1957) used by DiPrima & Stuart to parameterize the problem in terms of the bipolar radius $\rho \in [1, \beta]$, angle $\phi \in [0, 2\pi]$ and height $\zeta \in \boldsymbol{R}$. In the plane perpendicular to the ζ-axis, the coordinate system is transformed from conventional polar coordinates $z = r\exp i\theta$ to the modified bipolar coordinates $\omega = \rho \exp i\phi$ through the conformal transformation

$$z = \frac{a(\omega+\gamma)}{1+\gamma\omega},$$

where
$$\gamma = \frac{-(1+\beta)+[(1+\beta)^2-4\epsilon^2\beta]^{1/2}}{2\epsilon\beta},$$

$$\beta = 1+\alpha.$$

These coordinates have the advantage over conventional bipolar coordinates that they have a regular limit as $\epsilon \to 0$, allowing one to recover the concentric results. Figure 1 diagrammatically shows this coordinate system for eccentricity ϵ and radius ratio $\eta = a/b$ (which is approximately given by $\eta \sim 1/\beta$). The radial coordinate is non-dimensionalized by setting $\alpha = \beta - 1 = \delta(1-\epsilon^2)^{1/2}[1+O(\delta)]$ and

$$\rho = 1+\alpha(x+\tfrac{1}{2}).$$

The new radius variable $x \in [-\frac{1}{2}, \frac{1}{2}]$ corresponds to the inner cylinder at $x = -\frac{1}{2}$ and the outer at $x = \frac{1}{2}$.

The Jacobian that transforms Cartesian coordinates into this system is given by

$$J = \frac{(1+2\gamma\rho\cos(\phi)+\gamma^2\rho^2)^2}{(1-\gamma^2)^2} \tag{3.3}$$

and an element of length by

$$\mathrm{d}s^2 = a^2\left(\frac{1}{J}\mathrm{d}\rho^2 + \frac{\rho^2}{J}\mathrm{d}\phi^2 + \alpha^2\,\mathrm{d}\xi^2\right).$$

The height is typically scaled to give $\xi = \zeta/(a\alpha)$ and we will fix the periodicity in the ξ-direction to be of period $2\pi/\lambda$ for some λ, the axial wavenumber (to be determined) by defining the scaled height

$$z = \lambda\xi = \frac{\lambda}{a\alpha}\zeta.$$

Our starting point is the asymptotic expansion in powers of the eccentricity $\epsilon^{1/2}$ obtained by DiPrima & Stuart. Unfortunately, we cannot hope to include the details necessary to understand the derivation of the model, so we refer the reader to papers II and III.

DiPrima & Stuart assume that there are three small quantities: the relative gap α, the difference of the Taylor number from its critical value $T - T_c$ and the eccentricity ϵ. They perform the expansion in the region where the following relationship holds:

$$\alpha = 4k^2\epsilon^2$$

for k constant as $\epsilon \to 0$, and where the Taylor number is near the critical value T_0 (T_0 denotes the critical Taylor number at $\epsilon = 0$). We can non-dimensionalize the problem by setting the inner cylinder radius and the kinematic viscosity both to unity, by scaling time and space in the Navier–Stokes equations:

$$a = 1 \quad \text{and} \quad \nu = 1.$$

Thus the only parameters left in the problem are the eccentricity ϵ, k and the inner cylinder speed $Q = T_0^{1/2}\alpha^{-3/2}$ with the relationship

$$Q = \tfrac{1}{8}T_0^{1/2}k^{-3}\epsilon^{-3}. \tag{3.4}$$

The amplitude of the Taylor vortices scales like $\epsilon^{1/2}$, but we shall merely consider the amplitude of the Taylor vortices to be small and independent of ϵ and α.

3.3. *Solution for small eccentricity*

The asymptotic solution of the Navier–Stokes equations are given by (III, 2.9)–(III, 2.11) and expanded as in (III, 3.6)–(III, 3.8). After scaling the velocities by $1/Q$, we have:

$$u_\rho = \frac{\alpha}{2}\epsilon U(x,\phi) + \frac{1}{\alpha Q}\epsilon^{1/2} u_{TV},$$
$$u_\phi = \tfrac{1}{2}V(x,\phi) + \epsilon^{1/2} v_{TV},$$
$$u_\zeta = \frac{1}{\alpha Q}\epsilon^{1/2} w_{TV},$$

where

$$u_{TV} = u_0 + \epsilon^{1/2} u_1 + \ldots, \quad v_{TV} = v_0 + \epsilon^{1/2} v_1 + \ldots, \quad w_{TV} = w_0 + \epsilon^{1/2} w_1 + \ldots.$$

Now using the relationship between α, ϵ and Q we obtain

$$\left.\begin{aligned} u_\rho &= 2k^2\epsilon^3 U(x,\phi) + \frac{2k\epsilon^{3/2}}{T_0^{1/2}} u_{TV}, \\ u_\phi &= \tfrac{1}{2}V(x,\phi) + \epsilon^{1/2} v_{TV}, \\ u_\zeta &= \frac{2k\epsilon^{3/2}}{T_0^{1/2}} w_{TV}. \end{aligned}\right\} \tag{3.5}$$

The amplitude of the Taylor vortices is contained in the perturbation terms u_i, v_i and w_i.

3.4. *Eccentric Couette flow*

Before the onset of Taylor vortices, the perturbation of Couette flow by the eccentricity gives a two-dimensional flow that is described by the above equations with $u_i = v_i = w_i = 0$ and the functions U and V given by (III, 2.5), (III, 2.6)

$$\left.\begin{aligned} V &= V_0(x) + \epsilon V_1(x,\phi) + \epsilon^2 [V_{20}(x) + kT_0^{1/2} V_{21}(x,\phi) + 4k^2 V_{22}(x)] + O(\epsilon^3), \\ U &= U_0(x,\phi) + O(\epsilon), \end{aligned}\right\} \tag{3.6}$$

where (III, 2.7),

$$V_0 = 1-2x, \quad V_1 = 6(x^2-\tfrac{1}{4})\cos\phi, \quad V_{20} = 3(x^2-\tfrac{1}{4}),$$
$$V_{21} = (x^2-\tfrac{1}{4})[\tfrac{1}{3}(\tfrac{1}{20}-x^2) - \tfrac{2}{5}x(\tfrac{7}{12}-x^2)]\sin\phi, \quad V_{22} = x^2-\tfrac{1}{4}, \quad U_0 = 2(x^2-\tfrac{1}{4})(x-\tfrac{1}{2})\sin\phi.$$

3.5. *Taylor vortex flow*

The perturbed velocity fields including Taylor vortex effects are given by the functions u_i, v_i and w_i in (III, 3.6)–(III, 3.8).

The functions for $i = 0$ are given by (III, 4.1):

$$u_0 = -B(\phi) f_0(x)\cos z, \quad v_0 = B(\phi) g_0(x)\cos z, \quad w_0 = \lambda^{-1} B(\phi)\, \mathrm{D}f_0(x)\sin z, \tag{3.7}$$

where $\mathrm{D} = \mathrm{d}/\mathrm{d}x$. The functions f_0, g_0 are the solutions of the eigenvalue problem (II, 5.4)–(III, 5.6) with $\sigma = 0$; viz.

$$\left.\begin{aligned} &(\mathrm{D}^2-\lambda^2)^2 f_0 + \lambda^2 T_0 V_0 g_0 = 0, \\ &f_0 = (\mathrm{D}^2-\lambda^2) g_0 = 0, \\ &f_0 = \mathrm{D}f_0 = g_0 = 0 \quad \text{at} \quad x = \pm\tfrac{1}{2}, \end{aligned}\right\} \tag{3.8}$$

normalized so that $\mathrm{D}^3 f_0(-\frac{1}{2}) = 1$ (II, p. 407) and where the axial wavenumber λ is chosen to minimize T_0, i.e. at

$$T_0 = 1694.97, \quad \lambda = 3.127. \tag{3.9}$$

This is essentially the concentric stability problem; see (III, p. 94). From here on we shall assume that the parameters take these values. As described in §3.7, $B(\phi)$ comes from determining the higher-order approximations and using solutions to the adjoint problem of (3.8).

3.6. *Second order*

The next order of approximation is given by (III, 4.2):

$$\left.\begin{aligned} u_1 = -B^2(\phi) f_{12}(x)\cos 2z, \quad v_1 = v_{10}(x,\phi) + B^2(\phi)\, g_{12}(x)\cos 2z, \\ w_1 = (2\lambda)^{-1} B^2(\phi)\, \mathrm{D}f_{12}(x)\sin 2z. \end{aligned}\right\} \tag{3.10}$$

The functions f_{12}, g_{12} are the solutions of the non-homogeneous (regular) problem (III, 4.3)–(III,4.4):

$$\left.\begin{aligned} & f_{12} - (\mathrm{D}^2 - 4\lambda^2) g_{12} = \tfrac{1}{2}(f_0 \mathrm{D}g_0 - g_0 \mathrm{D}f_0), \\ & (\mathrm{D}^2 - 4\lambda^2)^2 f_{12} + 4\lambda^2 T_0 V_0 g_{12} = -f_0 \mathrm{D}^3 f_0 + (\mathrm{D}f_0)\mathrm{D}^2 f_0 - 2\lambda^2 T_0 g_0^2, \\ & f_{12} = \mathrm{D}f_{12} = g_{12} = 0 \quad \text{at} \quad x = \pm\tfrac{1}{2}. \end{aligned}\right\} \tag{3.11}$$

Furthermore, v_{10} is given by (III, 4.8)–(III, 4.12) and (III, 4.26*a*), (III, 4.30):

$$\left.\begin{aligned} & v_{10} = B^2(\phi)\, g_{10}(x) + \tfrac{1}{2}\sigma_0(x^2 - \tfrac{1}{4}), \quad g_{10}(x) = -\tfrac{1}{2}F_0(x) - 3Q_0(x^2 - \tfrac{1}{4}), \\ & F_0(x) = \int_{-1/2}^{x} f_0 g_0 \,\mathrm{d}x - (x + \tfrac{1}{2}) \int_{-1/2}^{1/2} f_0 g_0 \,\mathrm{d}x, \\ & Q_0 = \int_{-1/2}^{1/2} F_0(x)\,\mathrm{d}x, \quad \sigma_0 = \frac{3}{\pi} Q_0 \int_0^{2\pi} B^2(\phi)\,\mathrm{d}\phi. \end{aligned}\right\} \tag{3.12}$$

3.7 *The azimuthal dependence*

The function $B(\phi)$ necessary to complete the vector field described above is given by the integral of an equation of Bernoulli type. However, expanding $T = T_0 + \epsilon T_1 + \ldots$ (III, 3.4), in the limit $T_1 \to 0$, linearized theory gives an approximate solution (III, 5.6)

$$B^2(\phi) = A^2 \exp\left(\frac{\omega(\sin\phi - 1)}{k}\right) \tag{3.13}$$

with the constant $\omega = 1.122$ (III, 4.30) and A (written $B_0(k)$ in DiPrima & Stuart 1975) is an arbitrary constant, not determined in the linear approximation. This non-dimensional Taylor vortex amplitude A is proportional to $T_1^{1/2}$ for small T_1. Note that this approximation necessarily gives the maximum vortex activity 90° downstream of the large gap.

The normalization $\mathrm{D}^3 f_0(-\frac{1}{2}) = 1$ produces f_0, $\mathrm{D}f_0$ and g_0 of small amplitude:

$$\max_x |f_0| = 3.7 \times 10^{-3}, \quad \max_x |\mathrm{D}f_0| = 1.2 \times 10^{-2}, \quad \max_x |g_0| = 1.73 \times 10^{-4}.$$

Thus, comparing the amplitudes of V and v_{TV} at, for example, $\alpha = 0.097$ and $\epsilon = 0.1$, we find that they are of the same order when

$$A \sim 10^3,$$

indicating that the values of A used in §5 are moderate in the sense that the Taylor vortices can still be considered as a perturbation of the eccentric Couette flow. This scaling can be attributed to the large eigenvalue T_0 in equations (3.8).

4. Ensuring volume preservation

The flow field (3.5) is an approximate solution to the momentum equation (for a suitable pressure) and the continuity equation. The no-slip boundary conditions are exactly satisfied at each order. Since $\nabla \cdot \boldsymbol{u}$ is only approximately zero, fluid elements do not preserve their volume. In order to examine the motion of particles under the action of such a flow field, it is necessary that we construct a volume-preserving vector field Y with $\|Y-X\|$ small (we use the supremum norm) and the boundary conditions preserved, where X is the original vector field. The problem stems from the facts that the ϕ variable has a different order of magnitude to that of (x, z) and also the equation for volume conservation has a nonlinear dependence on ϵ. Truncating at any particular order will not guarantee exact volume preservation. The continuity equation in modified bipolar coordinates is

$$\frac{1}{\alpha}\frac{\partial}{\partial x}\left(\frac{\rho u_\rho}{J^{1/2}}\right)+\frac{\partial}{\partial \phi}\left(\frac{u_\phi}{J^{1/2}}\right)+\frac{\lambda}{\alpha}\frac{\partial}{\partial z}\left(\frac{\rho u_\zeta}{J}\right)=0. \tag{4.1}$$

We consider the problems for the underlying two-dimensional flow and the Taylor vortex flow separately.

In the following, we simplify the Jacobian by approximating the square root (3.3) expanding up to and including terms in ϵ^2. This has the form

$$\tilde{J}^{1/2} = 1+\epsilon\cos\phi+\frac{\epsilon^2}{2} \tag{4.2}$$

(cf. (III, 3.9)) and is consistent with the model of DiPrima & Stuart up to second order.

4.1. *The two-dimensional problem*

This was corrected by using the given function $V(x, \phi)$ to generate a streamfunction

$$\tilde{\psi} = -\int_{-1/2}^{x} \frac{V}{\tilde{J}^{1/2}}\,\mathrm{d}x \tag{4.3}$$

where terms of order higher than ϵ^2 in the integrand are ignored, and then the two modified velocity components are given by

$$\tilde{U}(x,\phi) = \frac{\tilde{J}^{1/2}}{\epsilon\rho}\frac{\partial\tilde{\psi}}{\partial\phi}, \tag{4.4}$$

$$\tilde{V}(x,\phi) = -\tilde{J}^{1/2}\frac{\partial\tilde{\psi}}{\partial x}. \tag{4.5}$$

Appendix A gives these expressions in full; note that they agree with the expressions obtained by DiPrima & Stuart up to second order.

4.2. *The Taylor vortex perturbations*

As noted in (III, p. 92), at second order the mean field $v_{10}(x, \phi)$ induces a modification to the radial velocity u_{30} to ensure the continuity equation is satisfied. Therefore, we first correct the radial component of the velocity by noting that

$$v_\rho = -\frac{J^{1/2}\alpha}{\rho}\int_{-1/2}^{x}\frac{\partial}{\partial\phi}\left(\frac{v_\phi}{J^{1/2}}\right)\mathrm{d}x \tag{4.6}$$

for a velocity field independent of z. Note that because we use a higher-order approximation to J than $J = 1$, extra terms at higher order than u_{30} are also created and these break the boundary condition at $x = \frac{1}{2}$. It is necessary to correct all terms using

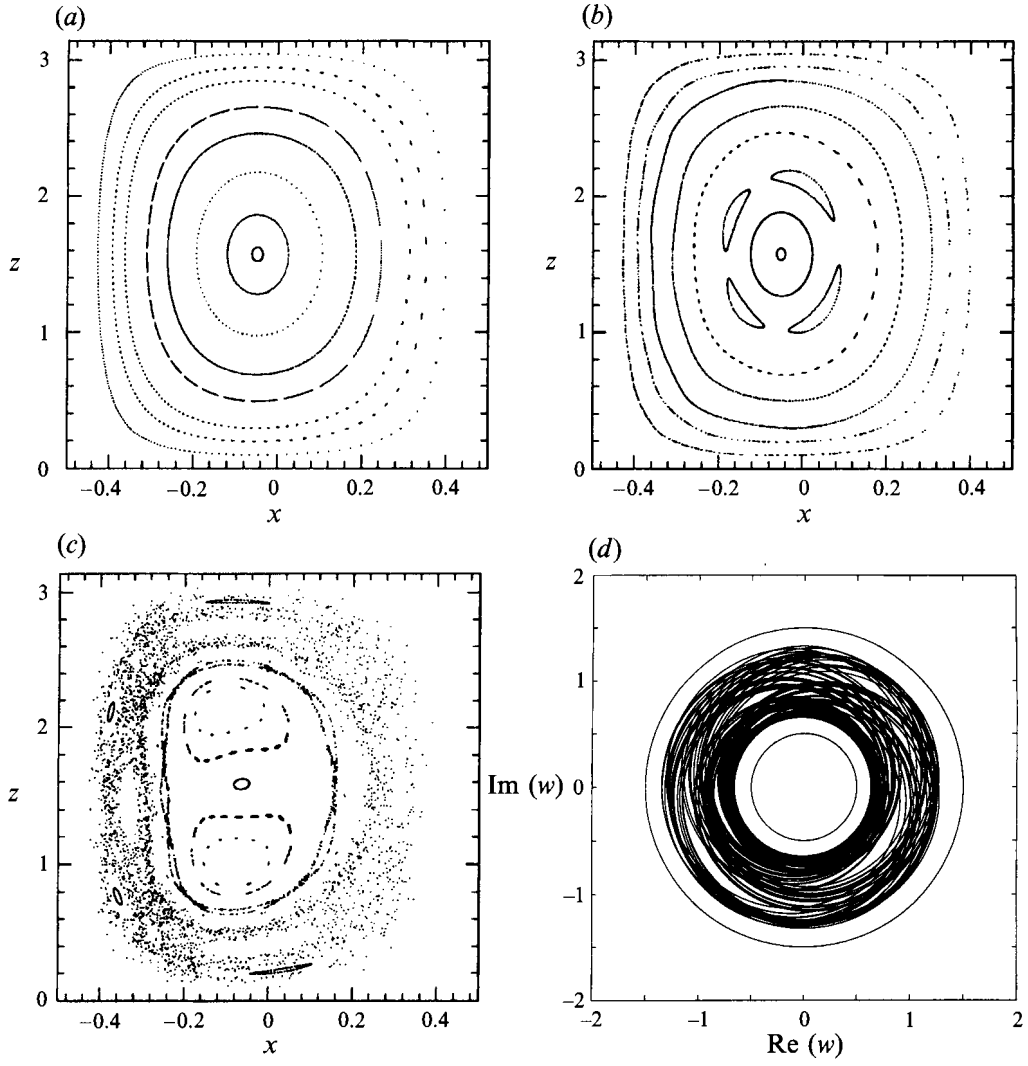

FIGURE 3. Mappings on the surface of section $\phi = 0$ (position of widest gap) and a representative trajectory for the first-order DiPrima & Stuart model. The outflow is at $z = 0$ and the inflow is at $z = \pi$. These figures show changes in the mapping for increasing Taylor vortex amplitude A in the case $\epsilon = 0.1$, $\delta = 0.096$. Between 600 and 1000 iterates are shown for each of 8 initial conditions. (*a*) $A = 100$: the flow is filled with KAM tori almost everywhere; the topology of the flow is very close to that for concentric Taylor vortices. (*b*) $A = 500$: a period-four Poincaré–Birkhoff island chain has been formed. (*c*) $A = 1000$: the islands near the edges of the vortex become smaller in size and there is a large stochastic layer. (*d*) Also at $A = 1000$: a representative trajectory is shown projected into the plane $w = (1+x)e^{i\phi}$. In this projection, the inner and outer cylinders appear as concentric circles and the gap between them is dilated.

the same approximation of J, otherwise we cannot expect to achieve exact preservation of any approximate volume.

The Taylor vortex perturbation terms other than v_{10} are corrected in the ζ component of the velocity using

$$v_\zeta = -\frac{J}{\rho\lambda}\int_0^z \frac{\partial}{\partial x}\left(\frac{\rho v_\rho}{J^{1/2}}\right)+\frac{\partial}{\partial\phi}\left(\frac{\alpha v_\phi}{J^{1/2}}\right)\mathrm{d}z. \tag{4.7}$$

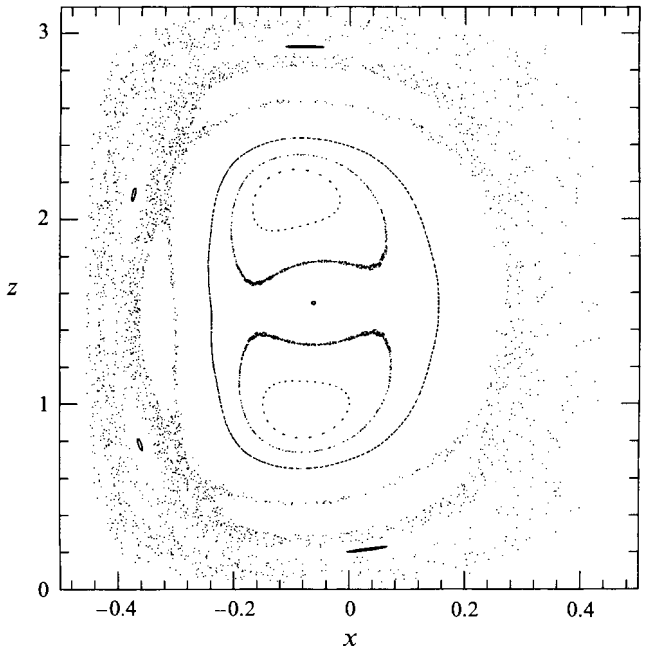

FIGURE 4. To compare with figure 3(*c*), this figure shows the second-order approximation of the DiPrima & Stuart model at the same surface of section and initial conditions, with $\epsilon = 0.1$, $\delta = 0.096$ and $A = 1000$. The similarity between this and the first-order approximation lends support to the existence of chaotic advection of the exact solution to the Navier–Stokes equations.

This introduces a small axially periodic correction term at the same order of perturbation as w_2 and ensures that the continuity equation is exactly satisfied. We denote the flow field corrected as above by $(\tilde{u}_\rho, \tilde{u}_\phi, \tilde{u}_\zeta)$.

The results displayed were obtained truncating at first order u_0 and v_0, except where indicated. We have performed particle tracking including the second-order terms derived by DiPrima & Stuart (u_1, v_1 and w_1). Even though the adjusted velocity field does not exactly satisfy the boundary condition at $x = \frac{1}{2}$ (although it does at $x = -\frac{1}{2}$ and in the ζ-direction) the results were very similar to those given in §5 even for moderately large ϵ and A (compare figures 3*c* and 4). No doubt there do exist perturbations of the second-order vector field that preserve all boundary conditions exactly, but we could not find a natural choice.

The differentiations and integrations outlined above were performed by an algebraic manipulation program to generate the optimized Fortran code necessary to evaluate the functions at any value of (x, ϕ, z) in the domain. The reason for using different corrections in the different components was to reduce the complexity and thus increase speed. Note that it would be unphysical to correct the given Couette flow by introducing a component in the z-direction, so we are forced to correct this flow in the (x, ϕ)-plane.

4.3. *Numerical method*

An approximation of the vector field was obtained by first solving the eigenvalue boundary value problem (3.8) to obtain Chebyshev polynomial representations of f_0, g_0, f_{12}, g_{12} and necessary (exact) integrals and differentials of these. The particle paths were then tracked for this approximated field.

The boundary value problems were solved using a Chebyshev series collocation

method (NAG routine D02JBF, Numerical Algorithms Group, Oxford, UK). The results were compared for calculations using between 10 and 20 collocation points in the radial direction; little qualitative difference was found in the results. The displayed results were calculated using 15 point collocation.

The particles were tracked by solving the following system of three first-order ordinary differential equations:

$$\dot{x} = \frac{\epsilon^{1/2}\tilde{J}^{1/2}\tilde{u}_\rho}{\alpha}, \quad \dot{\phi} = \frac{\epsilon^{1/2}\tilde{J}^{1/2}\tilde{u}_\phi}{\rho}, \quad \dot{z} = \frac{\epsilon^{1/2}\lambda\tilde{u}_\zeta}{\alpha}, \tag{4.8}$$

for given initial conditions. We have scaled $\tilde{u}$ by a factor of $\epsilon^{1/2}$ to ensure that these equations do not become singular as $\epsilon \to 0$; recall that $\alpha = O(\epsilon^2)$. A Runge–Kutta–Merson initial value solver with variable step-size (NAG routine D02BHF) was used to plot the intersections of the particle paths with the plane $\phi = 0$ (the largest gap between the cylinders).

5. The streamline topology

5.1. *Small eccentricity*

For eccentricities less than $\epsilon = 0.28$, there is no region of recirculation; u_ϕ is always positive for small enough A. As outlined in the introduction, we do not expect that the flow field should be completely integrable unless $\epsilon = 0$ due to the continuous symmetry group for the concentric case. Instead, the mapping on the surface of section $\phi = 0$ should be a generic map that preserves an area-form. We briefly review such predictions and refer the reader to Ottino (1989) and Arrowsmith & Place (1990) for more details.

The symmetry at $\epsilon = 0$ means that the Taylor vortices induce a mapping on a surface of section that is an integrable twist map, i.e. there is a central closed streamline about which all others turn at a variety of winding rates or numbers. About this central streamline, there is a set of nested stream tubes. The boundaries of these tubes intersect the surface of section at a set of nested invariant circles on which the winding number is constant. The winding number varies continuously according to which invariant circle one is on, and takes rational values on a dense set of these invariant circles. Fluid cannot be advected across these invariant circles. A generic perturbation which breaks the rotational symmetry of the concentric case will break the integrability of the twist map, and a variety of effects will become noticeable:

(i) Those invariant circles that are 'sufficiently irrational' in the sense of the KAM theorem will remain invariant until a finite level of perturbation from integrability is reached.

(ii) The invariant circles which have rational winding numbers will for $\epsilon > 0$ give pairs of alternating elliptic and hyperbolic periodic points. The map can be renormalized near the elliptic points to see the whole pattern again, on perturbing further from integrability.

(iii) The hyperbolic points created in (ii) will have stable and unstable manifolds that generically intersect transversely, creating chaotic horseshoe-like behaviour. The domain of this chaos is exponentially small for small perturbations but can expand to mix over almost the whole surface of section.

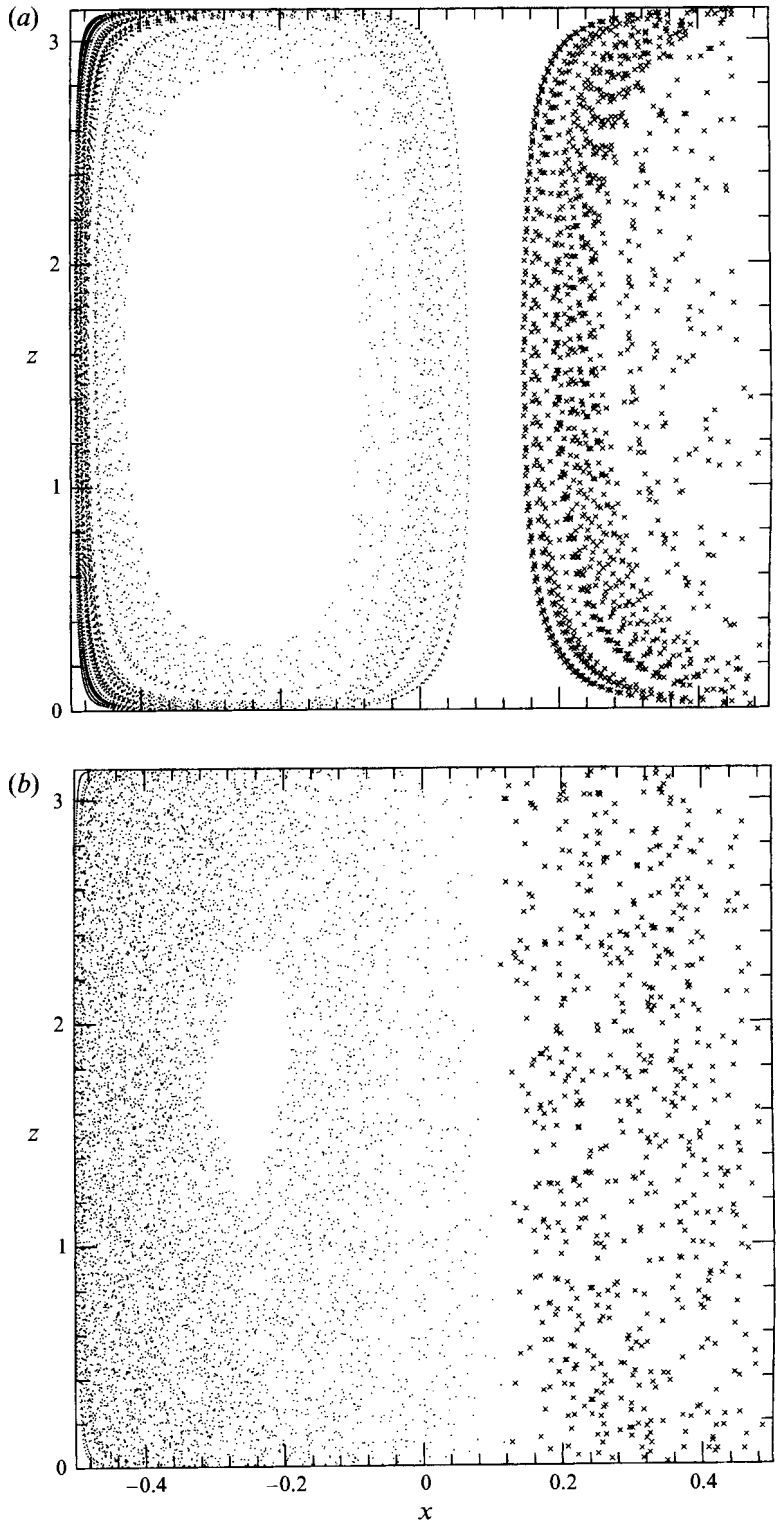

FIGURE 5(*a*, *b*). For caption see page 232.

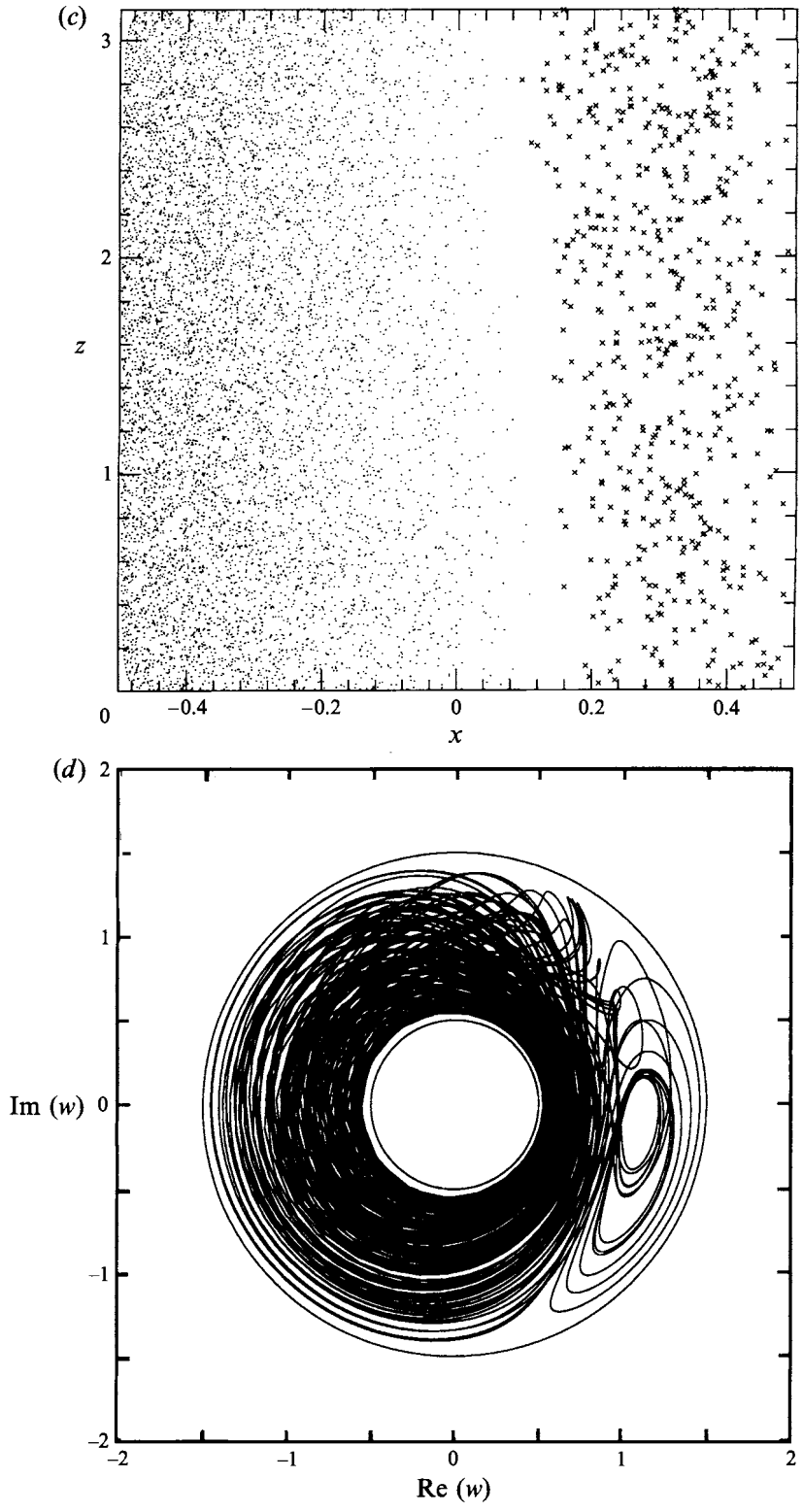

FIGURE 5(*c*, *d*). For caption see page 232.

5.1.1. *Chaotic streamlines*

Increasing the amplitude of the Taylor vortices A gives rise to a breakdown to chaos that is typical for area-preserving twist maps. This is illustrated in figure 3 for the case $\epsilon = 0.1, \delta = 0.096$. This figure shows the intersection of the streamlines with the surface $\phi = 0$ (the position of widest gap). At small amplitude (figure 3*a*, $A = 100$) the flow is filled with KAM tori almost everywhere; the topology of the flow is very close to that for Taylor vortices in concentric cylinders. On increasing A further (figure 3*b*, $A = 500$) there are seen to be four islands formed by the breakup of an invariant circle with rational winding number. Finally, we show for $A = 1000$ (figure 3*c*) that many of the KAM tori have broken up, leaving large areas of chaotic mixing interspersed with islands of no mixing. At the same parameter values, figure 3(*d*) shows a single representative trajectory projected into the $w = (1+x)e^{i\phi}$-plane. Figure 4 shows that on including the second-order terms in the expansion for the velocity field, there is a striking quantitative and qualitative similarity. This supports the conjecture that the chaotic mixing is not an artifact of the truncation.

5.2. *Large eccentricity*

As described earlier, a region of recirculation occurs when ϵ is increased past a critical value. Figure 5(*a–c*) shows the surface of sections for small-amplitude Taylor vortex flow with separation at $\epsilon = 0.5$; the amplitudes of the Taylor vortex motion are $A = 100$, $A = 500$ and $A = 1000$ respectively. In the basic two-dimensional flow the region of recirculation is defined by the dividing streamline. For the three-dimensional Taylor vortex flow one might naively suppose that the dividing streamline has become a dividing streamsurface and hence infer the existence of a separated vortex. Dynamical systems theory arguments suggest instead that there exist two important stream-surfaces. One of these surfaces is the unstable manifold emanating from the orbit connecting the separation points in the inflow and outflow, and the other surface is the stable manifold emanating from the orbit connecting the reattachment points in the inflow and outflow. In order to form a dividing streamsurface from these two surfaces, they must coincide. This will not occur generically; instead they will intersect one another transversely and so if they intersect once, then they intersect an infinite number of times, on one-dimensional sets. These intersections allow the streamlines to pass in and out of the recirculation region for all $A > 0$. Figure 5(*a–c*) verifies the correctness of the dynamical systems theory arguments. Note that in this figure, the region of backflow is indicated by crosses on the surface of section. Figure 5(*d*) shows (as in figure 3*d*) a single trajectory at $A = 1000$. The trajectory can be seen to enter and leave the region of recirculation in a chaotic manner.

For eccentricities large enough for separated flow to occur, it is no longer possible to claim that we are perturbing from an elliptic integrable situation as A increases. In

FIGURE 5. As in figure 3, but now with $\epsilon = 0.5$ (again $\delta = 0.096$). At this eccentricity there is separated two-dimensional flow when $T < T_c$ (i.e. $A = 0$). The crosses indicate the trajectory passing through the section in the negative ϕ-direction. Thus the region marked with crosses corresponds to the flow reversal part of the recirculation region. (*a*) $A = 100$. (*b*) $A = 500$. This section indicates that the mixing is very efficient except near the 'core' of the vortex. (*c*) $A = 1000$. There are no longer any signs of KAM surfaces in the section; most initial conditions mix throughout almost the whole of the vortex. Note the slight suppression of the recirculation in the neighbourhood of the outflow ($z = 0$) and its enhancement in the neighbourhood of the inflow ($z = \pi$). (*d*) Also at $A = 1000$: a representative trajectory that passes in and out of the recirculation region. As in figure 3(*d*), we have taken the projection $w = (1+x)e^{i\phi}$.

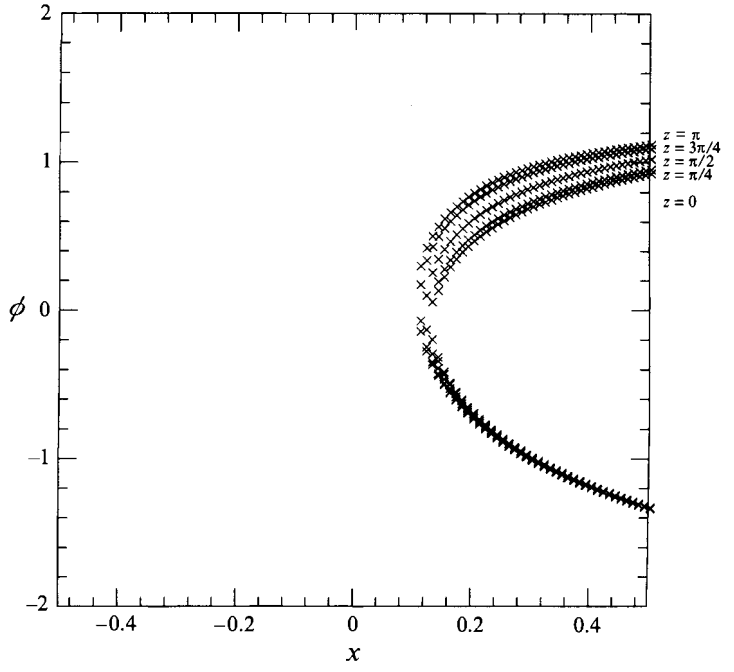

FIGURE 6. The zeros of the azimuthal velocity $u_\phi = 0$ are plotted in the (x, ϕ)-plane at five different z levels using the first-order truncation. $z = 0$ is the outflow, $z = \pi$ the inflow. These locations are obtained for $A = 1000$, $\epsilon = 0.5$ and $\delta = 0.096$. Note that the effect of the vortex amplitude is greatest downstream of the largest gap ($\phi \approx 1$ radian).

fact, at lower values of the Taylor vortex amplitude, there seem to be large regions of chaotic mixing. Note that as the Taylor vortex amplitude is increased, there is a tendency to enlarge the recirculation region in the inflow and shrink that in the outflow, as observed numerically by Dai *et al.* (1992) and experimentally by O'Brien *et al.* (1974). Figure 6 shows the location of flow reversal (i.e. $u_\phi = 0$) plotted in the (x, ϕ)-plane for five different levels of z going from the outflow ($z = 0$) to the inflow ($z = \pi$). This was computed for $\epsilon = 0.5$, $A = 1000$ with the first-order approximation. The enlargement of the recirculation in the inflow and reduction in the outflow is supported by numerical investigations, and also by observation of experiments in our laboratory. We now turn to this aspect of the flow geometry in more detail.

5.2.1. *Skin friction field*

In the region of parameter space where the recirculation region is created, we can use the model to describe the bifurcations and the fixed points they give rise to. To investigate the flow near the outer cylinder when this region is small, we use the skin friction field, defined on the outer cylinder $x = \frac{1}{2}$ by

$$w_\phi = -\frac{J^{1/2}}{\alpha}\frac{\partial u_\phi}{\partial x}, \quad w_z = -\frac{J^{1/2}}{\alpha}\frac{\partial u_z}{\partial x}.$$

The solution paths of the skin friction field give the streamlines for the model asymptotically close to the outer cylinder. Stagnation points on the boundary correspond to zeros of the skin friction field. The inflow and outflow boundaries have $w_2 = 0$ due to the reflection symmetry in their planes and so we can examine separation

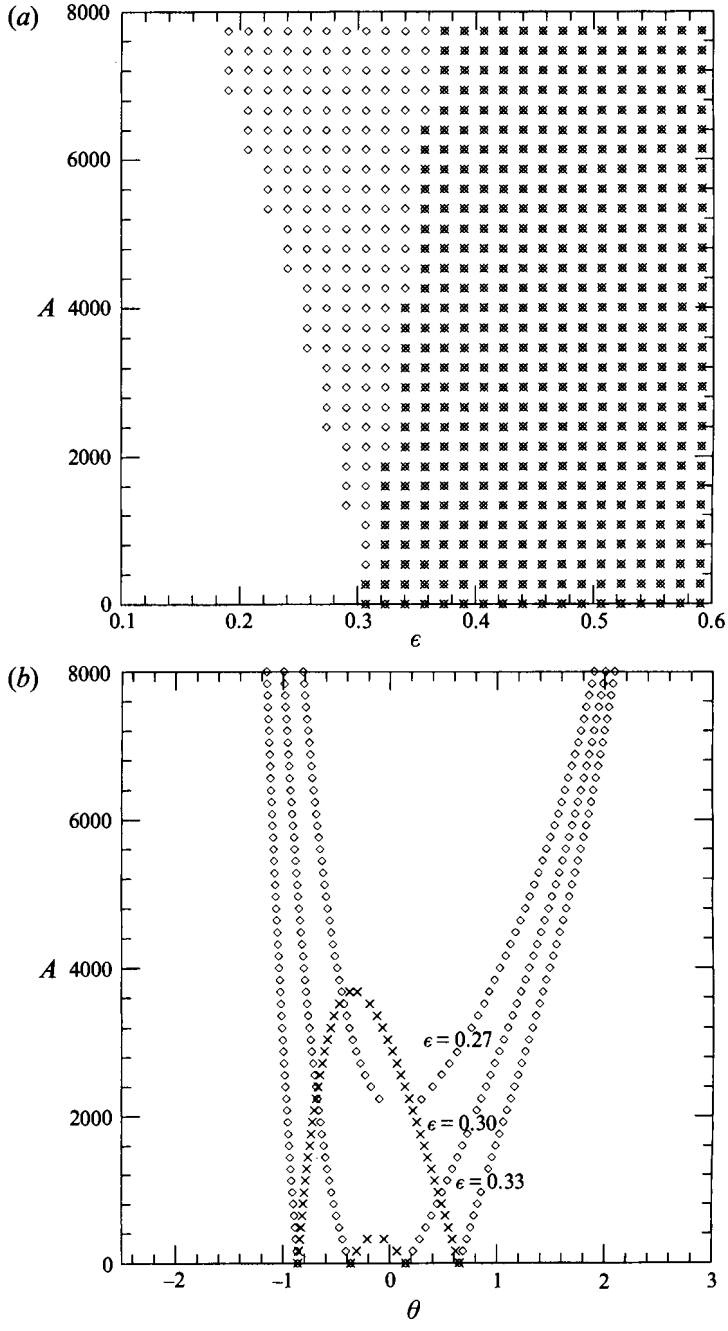

FIGURE 7. The dependence of the recirculation region on the Taylor vortex amplitude A, the eccentricity ϵ and the angle Θ around the outer cylinder for the first-order approximation is shown in these diagrams ($\delta = 0.096$). The point of widest gap is at $\Theta = 0$. The separation and reattachment points are found by searching for zeros in the azimuthal skin friction field in the in- and outflows. (*a*) Recirculation in the inflow (diamonds) and outflow (crosses) are shown as a function of A and ϵ. Note that there can be recirculation induced by the Taylor vortices for eccentricities lower than that required for separation in the two-dimensional flow. (*b*) The location of the separation points in the inflow (diamonds) and outflow (crosses) as a function of the Taylor vortex amplitude A. Three different eccentricities are shown. Note that for $\epsilon = 0.27$ there is no separation in the outflow and that separation in the inflow does not occur until $A > 2000$.

and reattachment points there by merely computing roots of $w_\phi = 0$ in these planes. Figure 7 shows the results for several eccentricities and a range of Taylor vortex amplitudes for first-order approximations; the corresponding results for second order are shown in figure 8. The angle Θ is the angle measured from the centre of the outer cylinder, with $\Theta = 0$ at the largest gap; this was computed using equation (II, 6.17). As is apparent from this figure, the DiPrima & Stuart model predicts that the recirculation region in the inflow is enlarged by imposing low-amplitude Taylor vortex motion while the recirculation in the outflow is reduced. These results offer an explanation for the observation by Koschmieder (1976) of flow separation for $T > T_c$ at lower ϵ than necessary for separation in two-dimensional flow ($T < T_c$). Although he did not elaborate on whether the observed 'premature' separation was in both inflow and outflow, we suggest that separation probably did not occur in the outflow.

Collecting the results for large eccentricity (but small Taylor vortex amplitude) we conclude that the stagnation points in the fluid and on the skin friction field connect together to give a flow skeleton (MacKay 1994). This is shown in figure 9. The interconnecting orbits transversely intersect in the generic case, implying the existence of chaotic streamlines near them.

5.3. *Premature separation*

In this section we offer an explanation for the premature flow separation in the outflow, described above. As Prandtl (1905) first observed, a small amount of suction can prevent or delay separation. Since the outflow jet imparts a component of the velocity normal to the wall, we suggest that the outflow jet acts much like wall suction and hence will tend to suppress separation. Conversely the inflow jet acts like 'blowing' and hence will promote separation. We make this idea clearer by examining the Taylor vortex perturbation in the ϕ component of the skin friction field. This is given (after scaling by $J^{1/2}/\alpha$) by

$$w_\phi = -\epsilon^{1/2}\frac{\partial V}{\partial x} - \epsilon B(\phi)\frac{\mathrm{d}g_0}{\mathrm{d}x}\cos z,$$

where x is taken to be $\frac{1}{2}$, the outer boundary. Consider an eccentricity ϵ_0 such that Couette flow is about to separate at, say $\phi = \phi_0$. This means that for $B(\phi) = 0$ we have $w_\phi = \partial w_\phi/\partial\phi = 0$, $K_1 = \partial^2 w_\phi/\partial\phi^2 > 0$ and $K_2 = \partial w_\phi/\partial\epsilon < 0$ at $\phi = \phi_0$ and $\epsilon = \epsilon_0$. Thus, expanding $\partial V/\partial x$ as a Taylor series we get

$$-\frac{\partial V}{\partial x} = K_1(\phi-\phi_0)^2 + K_2(\epsilon-\epsilon_0)$$

to lowest order jointly in $\epsilon-\epsilon_0$ and $\phi-\phi_0$. Thus stagnation points ϕ satisfy

$$0 = K_1(\phi-\phi_0)^2 + K_2(\epsilon-\epsilon_0) + K_3 A\epsilon_0^{1/2}\cos z \tag{5.1}$$

for small $\epsilon-\epsilon_0$ and $\phi-\phi_0$. Numerically, we have that $\mathrm{d}g_0/\mathrm{d}x < 0$ at $x = \frac{1}{2}$ implying that $K_3 > 0$. From this equation it is clear that the effective ϵ_0 is decreased in the inflow ($z = \pi$), while it is increased in the outflow ($z = 0$). Equation (5.1) describes a saddle-node bifurcation of the skin friction field on the planes of the inflow and outflow boundaries.

We also note that near the endplates of an experimental apparatus, fluid is driven inward toward the rotating cylinder. By the argument above, this should promote recirculation in the inflows. Thus in long cylinder systems we expect the inflows of the vortices near the ends to be more prone to recirculation than in the middle of the cylinders. This effect will be even more pronounced for short cylinders. This has indeed

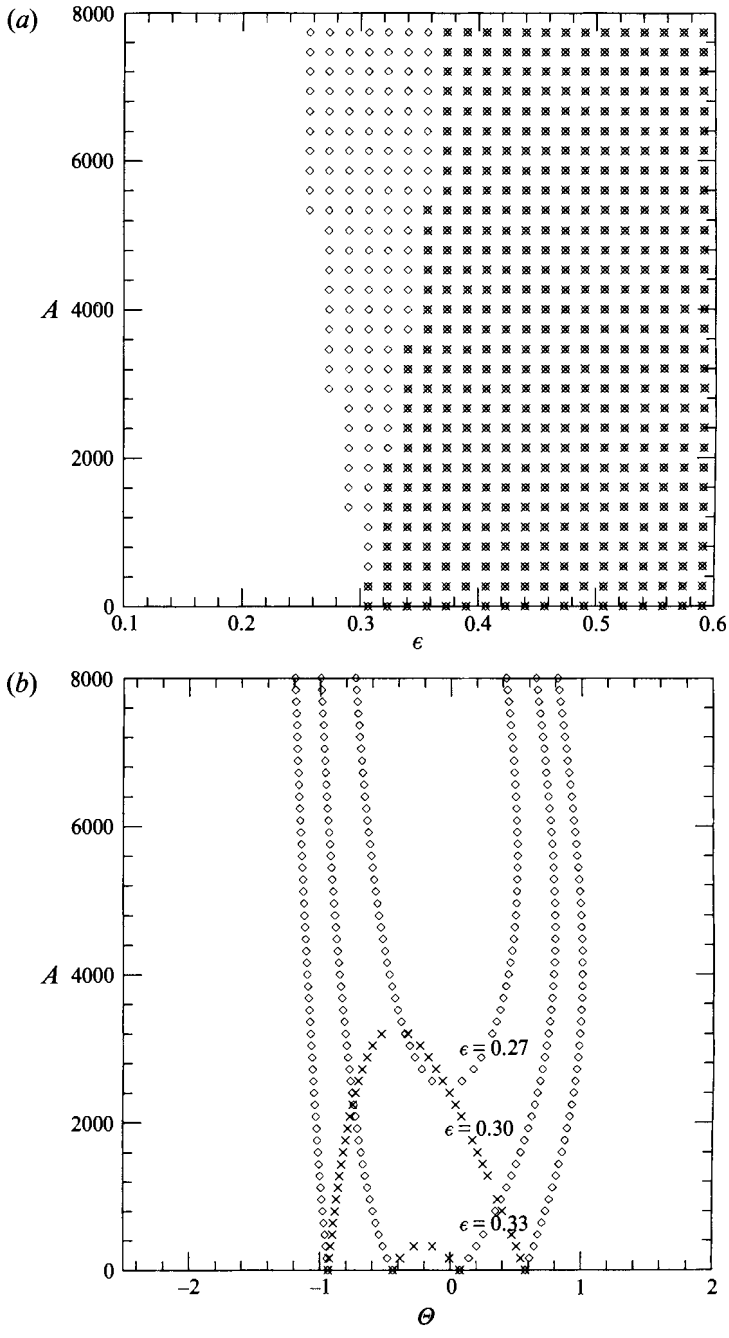

FIGURE 8. As in figure 7, but this time using the second-order approximation. (*a*) The second-order terms cause a perturbation of the boundaries of the regions of existence of the recirculation regions. (*b*) Viewed in the (a, Θ)-plane, the presence of second-order terms perturbs the positions of the in- and outflows at larger values of A.

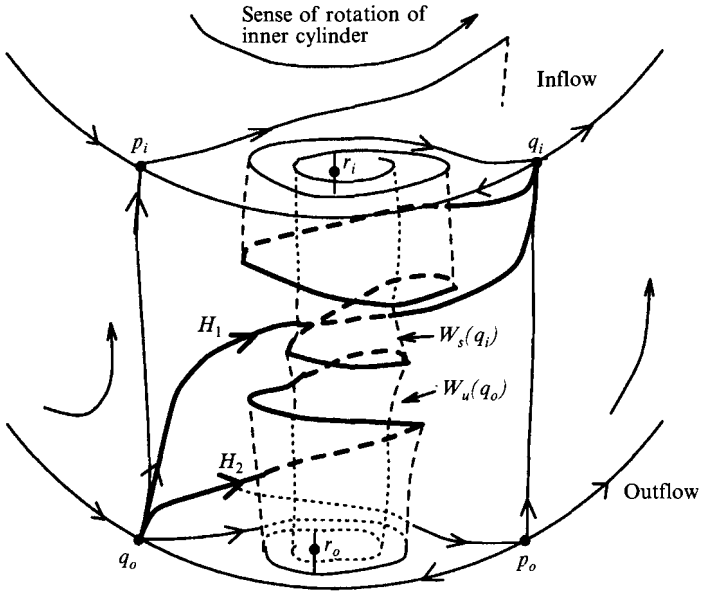

FIGURE 9. The 'flow skeleton' for small-amplitude Taylor vortex flow with separation. The flow skeleton consists of the fixed point of the flow and skin friction fields together with some of their connecting orbits. There are two skin friction saddle points, q_o and q_i and a source and sink p_o, p_i. The flow lines to the left and right of the recirculation region are for the skin friction field. In the fluid there are saddle spiral stagnation points at r_o, r_i. The bold lines H_1 and H_2 are heteroclinic connections from q_o to q_i. Note that the unstable manifold $W_u(q_o)$ and the stable manifold $W_s(q_i)$ are only partially drawn. In fact there are infinitely many heteroclinic orbits from q_o to q_i; $W_u(q_o)$ and $W_s(q_i)$ will intersect each other in a complicated manner. As can be seen from the diagram, there is no unique choice for a 'separating surface'; in fact there will be streamlines that pass in and out of the recirculation region for all non-zero A.

been found to be the case in our laboratory and in recent numerical investigations (Szeri & Al-Sharif 1993).

6. Discussion

Throughout this investigation we have taken the approach that we wish to find the simplest asymptotic model such that we can obtain answers to questions about the geometry of the flow field. Unfortunately, the stronger chaotic mixing occurs only when we perturb away from the integrable concentric case, precisely when the convergence of the asymptotic expansion can be called into question. However, the fact that the addition of second-order terms only slightly perturbs the flow patterns suggests that the predictions are valid.

Particularly important is the modification made to ensure volume preservation. It is easy to adjust a vector field to ensure this, but simultaneously preserving the boundary conditions is a more difficult matter. We only managed to achieve both for the first-order approximation. We could only find perturbations of the second-order terms which either involve an aperiodic term in u_ζ or break the boundary conditions on u_ρ (at high order).

The stability or otherwise of these solutions do not concern us here. It is of course the case that for small enough eccentricities the bifurcation to Taylor vortices is supercritical (giving rise to stable vortex structure) but the case for large eccentricities (such that there is recirculation) is not known; the DiPrima & Stuart model predicts

supercritical bifurcation, but the region of validity is not known. Even disregarding the stability question, we feel that the results we have obtained are interesting from the point of view of showing that there are mixing streamlines even for time-independent flows close to Taylor vortex flow.

6.1. *A modulated vortex model*

It is important to develop an understanding of the physics which controls the breakup of the streamlines. With this objective in mind, we have investigated a simplified model of the mechanism by which the mixing occurs in the unseparated (small ϵ) limit. The vector field defined by the DiPrima & Stuart model can be thought of as a vortex encircling the cylinder that is periodically modulated in the azimuthal direction (the function $B(\phi)$ represents this modulation). Thus, we unwrap the cylinder and model the flow as a vortex with streamfunction ψ_1 periodically perturbed by a vortex pair with streamfunction ψ_2. These two-dimensional streamfunctions in the (x, z)-plane and are given by

$$\psi_1(x,z) = \sin x \sin z, \quad \psi_2(x,z) = \sin 2x \sin z,$$

where x, z and ϕ are as in the DiPrima & Stuart model. We define the following volume-preserving field:

$$\left.\begin{aligned} v_x &= \frac{\partial \psi_1}{\partial z}(1-\lambda(\phi)) + \frac{\partial \psi_2}{\partial z}\lambda(\phi), \\ v_\phi &= 1, \\ v_z &= -\frac{\partial \psi_1}{\partial x}(1-\lambda(\phi)) - \frac{\partial \psi_2}{\partial x}\lambda(\phi). \end{aligned}\right\} \tag{6.1}$$

There are invariant surfaces at $x, z = 0, \pi$ for all ϕ and so we restrict to the box $(x, z) \in [0, \pi]^2$. We take

$$\lambda(\phi) = \epsilon \cos^2 \phi.$$

The streamfunction ψ_1 defines a flow on the (x, z)-plane which consists of a single vortex in the region studied. The function $\lambda(\phi)$ modulates this with a deformation ψ_2 which moves the centre of the vortex periodically from side to side, in the x-direction. The case $\epsilon = 0$ is integrable, and increasing ϵ away from zero breaks this integrability. This flow neither satisfies the Navier–Stokes equations nor any no-slip boundary conditions but has the same qualitative features, i.e. that of a generic area-preserving map. In fact equation (6.1) can be seen as a time-dependent one degree of freedom Hamiltonian system. In Appendix B of this paper, Professor George Rowlands shows how a Poincaré map valid for small ϵ can be constructed for model (6.1) which exhibits the basic features shown in figure 10. The principal importance of the map is that it shows that the physics is controlled by a single parameter which is a given function of the winding number of the invariant circles in the $\epsilon = 0$ case.

6.2. *Transport*

In this paper we have concentrated on the transport of fluid elements within a vortex, and it is clear from our investigations that the presence of a region of recirculation yields much stronger mixing than the weakly eccentric limit. We find that when the region of recirculation exists, most chaotic mixing occurs near MacKay's flow skeleton.

For a real system with no-slip boundary conditions on the endplates, MacKay (1994) has noted that there will be transport of particles between adjacent vortices,

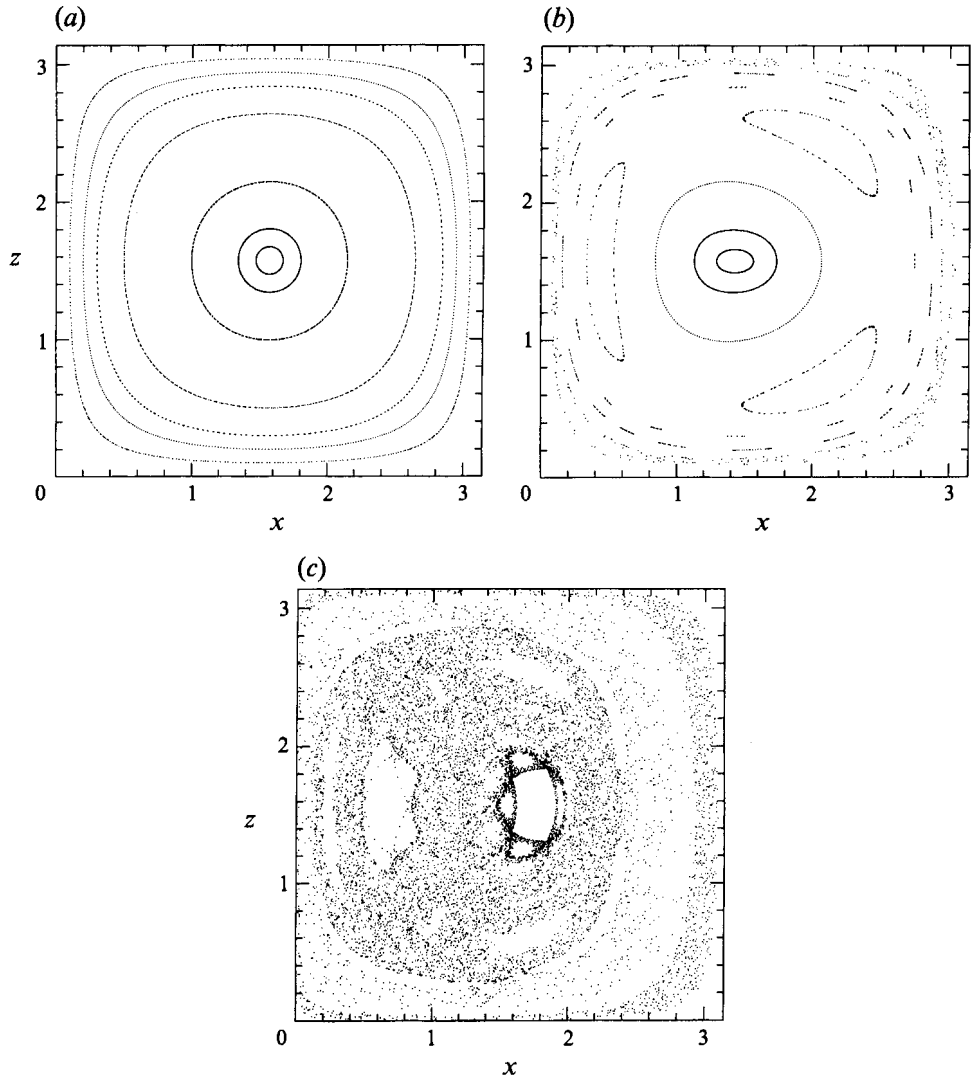

FIGURE 10. For the modulated vortex model (6.1) these figures show results at differing levels of ϵ, the perturbation from integrability. In each case, the orbits of seven different initial conditions are shown. (*a*) The integrable case, $\epsilon = 0$. (*b*) $\epsilon = 0.4$; a period three island chain is prominent. (*c*) $\epsilon = 0.6$; most KAM tori have now been destroyed, permitting diffusion of streamlines throughout most of the fluid.

even for the case of no diffusion. This is because of the destruction of the invariant planes $z = 0$ and $z = \pi$ in the model (the translational symmetry in the z-direction is destroyed). However, for long cylinders we expect the mixing in and out of the recirculation region to be dominant over inter-vortex mixing, at least near the centre of the apparatus.

By analogy with the concentric case, Taylor vortices are expected to go unstable to wavy vortices when a certain Taylor vortex amplitude is reached. This instability has been investigated theoretically by Weinstein (1977*a*, *b*) and experimentally by Vohr (1968), Cole (1965, 1976), Ozogan & Mobbs (1980), and Zarti & Mobbs (1980). For wavy vortex flows enhanced mixing is expected, effectively due to the creation of a

four-dimensional volume-preserving system. However, MacKay (1994) notes that there may still be three-dimensional obstructions to the transport of fluid throughout the system. One possible extension of the present work is to investigate inter-vortex mixing using Weinstein's asymptotic model.

7. Conclusions

In addition to the possible extensions of this work that we have already discussed, we emphasize that we have only just scratched the surface of the asymptotic model of DiPrima & Stuart. There remain many interesting predictions of the model yet to be discovered and this can provide an impetus for further numerical and experimental work on the eccentric rotating cylinders problem. In particular it would be interesting to collect some experimental observations of the recirculation and chaotic streamlines that we have observed numerically. One direction for further work is to use the expression for Taylor vortex amplitude $B(\phi)$ from the nonlinear theory DiPrima & Stuart (1975), Eagles *et al.* (1978), which would give more accurate quantitative predictions of separation. However by the genericity argument already outlined we do not expect that introducing higher-order approximations would remove the presence of e.g. chaotic advection in the Taylor vortices. The ensuring of volume preservation was performed using an *ad hoc* method; work is in progress to find more efficient and generally applicable methods.

Practically, our methods would be just as applicable to the case $q_2 \neq 0$, the outer cylinder rotating as well. In this case we could investigate the possibility of Taylor vortex instability of the two-dimensional flow with recirculation zones in the interior of the flow (see figures 14–16 in Ballal & Rivlin 1977).

In the introduction we pointed out that a major source of concern is the worry that the bifurcations in the streamline topology of the truncated equations may not be related in any qualitative way to the actual transitions in the fluid. This is certainly the case for the Lorenz equations as a model of Rayleigh–Bénard convection. The source of the problem there was investigated in depth by Marcus (1981) who identified the physically important process (boundary-layer behaviour) which the Lorenz-type models failed to model sufficiently well. In the present case, a similar study would be of considerable value.

Final remark

We end this paper with the following remark. The dynamical system which determines the streamlines can be thought of as being hierarchical; this is a dynamical system determined by the Navier–Stokes equations which evolves towards a fixed flow field. This flow field determines the streamlines; a change in parameters may distort the velocity field but not give rise to a bifurcation to a different flow pattern. Nevertheless, changes in parameters can lead to bifurcations in the dynamics of the streamlines. Whether this view can be exploited to obtain a deeper understanding of stability and transition of the flow patterns themselves, remains to be discovered.

Thanks are due to Kryzstof Banas, Tom Bridges, Alison Cooper, Philip Drazin, Paul Duineveld, Norbert Ligterink, Jeroen Nijhof, John Phelps, Robert MacKay, David Rand, George Rowlands, Chris Shaw and J. T. Stuart for conversations which contributed to our understanding of this system. We thank the SERC Nonlinear Initiative for support during this research and the referees for their valuable comments.

Appendix A. The modified equations

Expressions for the volume-conserving modification to the two-dimensional flow are given by

$$\begin{aligned}\tilde{U}(x,\phi) = &-((2x+1)(2x-1)^2\\ &\times(8\epsilon k\,T_0^{1/2}\cos(\phi)\,x^3-4\epsilon k\,T_0^{1/2}\cos(\phi)\,x^2-10\epsilon k\,T_0^{1/2}\cos(\phi)\,x\\ &-480\epsilon\cos(\phi)\sin(\phi)-240\sin(\phi)-3k\,T_0^{1/2}\cos(\phi)\,\epsilon)\\ &\times(2-2\cos(\phi)\,\epsilon+\epsilon^2))/(1920+7680\epsilon^2k^2x+3840k^2\epsilon^2),\\ \tilde{V}(x,\phi) = &(2x-1)(48\epsilon^2k\,T_0^{1/2}\sin(\phi)\,x^4-16\epsilon^2k\,T_0^{1/2}\sin(\phi)\,x^3\\ &-48\epsilon^2k\,T_0^{1/2}\sin(\phi)\,x^2+720\epsilon^2\cos(\phi)^2x+480\epsilon^2k^2x+360\epsilon^2x\\ &+720\epsilon\cos(\phi)\,x-12\epsilon^2kT_0^{1/2}\sin(\phi)\,x+120\cos(\phi)\,\epsilon+120\epsilon^2\cos(\phi)^2\\ &+\epsilon^2k\,T_0^{1/2}\sin(\phi)-240+300\epsilon^2+240k^2\epsilon^2)(2-2\cos(\phi)\,\epsilon+\epsilon^2)/480.\end{aligned}$$

Routine calculations show that these agree with the original expressions (III, 2.5), (III, 2.6), (III, 2.7) up to and including terms of $O(\epsilon^2)$.

Appendix B. Approximation of the return map for the modulated vortex model

By G. Rowlands
Department of Physics, University of Warwick, Coventry CV4 7AL, UK

In the case of small ϵ one can analytically construct a Poincaré map approximating the return map of (6.1) which exhibits the basic features shown in figure 10. The principal importance of the map is that it shows that the physics is controlled by a single parameter which is a given function of the winding number of the invariant circles (stream tubes) in the $\epsilon = 0$ case.

The method of obtaining the map is similar to that used in plasma physics to study the motion of charged particles in spatially non-uniform magnetic fields. In that context the system is described by a quantity μ, a so-called adiabatic invariant, which is essentially the local magnetic moment associated with the gyro-magnetic rotation of the charged particle, and an angle θ known as the Larmor phase angle. In the present case the role of the adiabatic invariant is the streamfunction $\psi_1 = \sin x \sin z$ and the phase angle is ϕ – a time-like variable.

In the aforementioned case of the motion of charged particles, it is well understood that the reason one gets chaos is the resonance between the Larmor frequency ω_L and a frequency associated with the non-uniformity of the magnetic field ω_N (Lichtenberg & Lieberman 1982). Chirikov (1979) has studied this resonance behaviour in general Hamiltonian systems and has shown how these systems can, with suitable approximations, be reduced to a study of simple maps. In the present problem ω_L corresponds to the frequency of the streamlines winding around a stream tube, and ω_N corresponds to the modulation in ϕ which here is equal to 1.

We can rewrite equations (6.1) in the form

$$\left.\begin{aligned}\frac{\mathrm{d}x}{\mathrm{d}\phi} &= \sin x\cos z\{1-\epsilon\lambda(\phi)[1-2\cos x]\},\\ \frac{\mathrm{d}z}{\mathrm{d}\phi} &= -\cos x\sin z\left\{1-\epsilon\lambda(\phi)\left[1-\frac{2\cos 2x}{\cos x}\right]\right\},\end{aligned}\right\} \tag{B 1}$$

and define an effective time τ such that

$$\frac{d\tau}{d\phi} = 1-\epsilon\lambda(\phi)[1-2\cos x]$$

in which case equations (B 1) reduce to

$$\frac{dx}{d\tau} = \sin x \cos z,$$

$$\frac{dz}{d\tau} = -\cos x \sin z + 2\epsilon\lambda(\phi)\sin z \sin^2 x + O(\epsilon^2).$$

These equations may be solved using a multiple time perturbation theory asymptotic as $\epsilon \to 0$. Thus we introduce two times $\tau_0 = \tau$ and $\tau_1 = \epsilon\tau$, treat them as independent variables and formally expand x and z as follows (cf. Rowlands 1990):

$$x = x_0(\tau_0, \tau_1) + \epsilon x_1 + \ldots, \quad z = z_0(\tau_0, \tau_1) + \epsilon z_1 + \ldots.$$

At order ϵ^0 we get

$$\frac{dx_0}{d\tau_0} = \sin x_0 \cos z_0, \quad \frac{dz_0}{d\tau_0} = -\cos x_0 \sin z_0,$$

which may be rewritten in the form

$$K_0 = \sin x_0 \sin z_0 \quad \text{(a constant)},$$

and

$$\left(\frac{dx_0}{d\tau_0}\right)^2 = \sin^2 x_0 - K_0^2.$$

This gives

$$\sin x_0 = \mathrm{dn}(\tau_0 + \psi, k_0)$$

where $\mathrm{dn}(x, k)$ is a Jacobian elliptic function, $k_0^2 = 1 - K_0^2$ and both the phase factor ψ and k_0 must be considered to be functions of τ_1. To order ϵ^1 we get

$$\frac{dx_1}{d\tau_0} - (\cos x_0 \cos z_0)\, x_1 + K_0 z_1 = -\frac{dx_0}{d\tau_1},$$

$$\frac{dz_1}{d\tau_0} + (\cos x_0 \cos z_0)\, z_1 - K_0 x_1 = -\frac{dz_0}{d\tau_1} + 2\lambda(\phi)\sin z_0 \sin^2 x_0.$$

Eliminating z_1 from the two equations gives

$$\frac{d^2 x_1}{d\tau_0^2} - (\cos 2x_0)\, x_1 = -\left(\frac{d}{d\tau_0} + \cos x_0 \cos z_0\right)\frac{dx_0}{d\tau_1} + K_0 \frac{dz_0}{d\tau_1} - 2\lambda(\phi) K_0 \sin^2 x_0 \sin z_0,$$

and using the equation for $dx_0/d\tau_0$ finally gives

$$\frac{d^2 x_1}{d\tau_0^2} - (\cos 2x_0)\, x_1 = 2\left\{K_0 \frac{dz_0}{d\tau_1} - \cos x_0 \cos z_0 \frac{dx_0}{d\tau_1}\right\} - 2\lambda(\phi) K_0^2 \sin x_0.$$

Since

$$\frac{d^2}{d\tau_0^2}\left(\frac{dx_0}{d\tau_0}\right) - \cos 2x_0 \frac{dx_0}{d\tau_0} = 0$$

and x_0 is periodic with period T, if we demand that x_1 is also periodic in τ_0 then we have

$$\int_0^T \left\{ K_0 \frac{\mathrm{d}z_0}{\mathrm{d}\tau_1} - \cos x_0 \cos z_0 \frac{\mathrm{d}x_0}{\mathrm{d}\tau_1} \right\} \frac{\mathrm{d}x_0}{\mathrm{d}\tau_0} \mathrm{d}\tau_0 = K_0^2 \int_0^T \lambda(\phi) \sin x_0 \frac{\mathrm{d}x_0}{\mathrm{d}\tau_0} \mathrm{d}\tau_0.$$

Since K_0 is constant on the τ_0 time scale.

We allow ψ and k_0, which appear in $\sin x_0$, to be functions of τ_1. With $\sin x_0 = \mathrm{dn}(\tau_0 + \psi, k_0)$ we find that

$$K_0 \frac{\mathrm{d}z_0}{\mathrm{d}\tau_1} - \cos x_0 \cos z_0 \frac{\mathrm{d}x_0}{\mathrm{d}\tau_1} = -\frac{\mathrm{d}}{\mathrm{d}\tau_1}(\sin x_0 \cos z_0) = -\frac{\mathrm{d}}{\mathrm{d}\tau_1} \frac{\mathrm{d}x_0}{\mathrm{d}\tau_0},$$

since $K_0 = \sin x_0 \sin z_0$. Thus our consistency condition takes the form

$$-\frac{1}{2} \int_0^T \frac{\mathrm{d}}{\mathrm{d}\tau_1} \left(\frac{\mathrm{d}x_0}{\mathrm{d}\tau_0} \right)^2 \mathrm{d}\tau_0 = -K_0^2 \int_0^T \lambda(\phi) \frac{\mathrm{d}}{\mathrm{d}\tau_0} (\cos x_0) \mathrm{d}\tau_0.$$

On the right-hand side we may replace $\lambda(\phi)$ by $\lambda(\tau_0)$ to lowest order and if the integration over τ_0 is between zeros of $(\mathrm{d}x_0/\mathrm{d}\tau_0)^2$, we have

$$\frac{\mathrm{d}}{\mathrm{d}\tau_1} \left(\int_0^T \left(\frac{\mathrm{d}x_0}{\mathrm{d}\tau_0} \right)^2 \mathrm{d}\tau_0 \right) = 2K_0^2 \int_0^T \lambda(\tau_0) \frac{\mathrm{d}}{\mathrm{d}\tau_0} (\cos x_0) \mathrm{d}\tau_0. \tag{B 2}$$

The integral on the left-hand side will be independent of ψ but is a function of k_0 so

$$\frac{\mathrm{d}}{\mathrm{d}\tau_1} \to \frac{\mathrm{d}k_0}{\mathrm{d}\tau_1} \frac{\mathrm{d}}{\mathrm{d}k_0}.$$

Recalling that $K_0^2 = 1 + k_0^2$, the left-hand side then gives

$$\begin{aligned} \frac{\mathrm{d}k_0}{\mathrm{d}\tau_1} \frac{\mathrm{d}}{\mathrm{d}k_0} \left(\int_0^T \left(\frac{\mathrm{d}x_0}{\mathrm{d}\tau_0} \right)^2 \mathrm{d}\tau_0 \right) &= 2 \frac{\mathrm{d}k_0}{\mathrm{d}\tau_1} \frac{\mathrm{d}}{\mathrm{d}k_0} \left(\int_{x_0^{(1)}}^{x_0^{(2)}} (\sin^2 x_0 - K_0^2)^{1/2} \mathrm{d}x_0 \right) \\ &= -\frac{\mathrm{d}k_0}{\mathrm{d}\tau_1} \frac{k_0}{K_0} 2 \frac{\mathrm{d}}{\mathrm{d}K_0} \int_{x_0^{(1)}}^{x_0^{(2)}} (\sin^2 x_0 - K_0^2)^{1/2} \mathrm{d}x_0 \\ &= 2k_0 \frac{\mathrm{d}k_0}{\mathrm{d}\tau_1} \int_{x_0^{(1)}}^{x_0^{(2)}} \frac{\mathrm{d}x_0}{(\sin^2 x_0 - K_0^2)^{1/2}} \end{aligned}$$

where $\mathrm{d}x_0/\mathrm{d}\tau = 0$ for $x_0 = x_0^{(1),(2)}$. But

$$T = \int_0^T \mathrm{d}\tau_0 = 2 \int_{x_0^{(1)}}^{x_0^{(2)}} \frac{\mathrm{d}x_0}{(\sin^2 x_0 - K_0^2)^{1/2}}$$

so that (B 2) reduces to

$$\frac{\mathrm{d}k_0^2}{\mathrm{d}\tau_1} = \frac{4K_0^2}{T} \int_0^T \lambda(\tau_0) \frac{\mathrm{d}}{\mathrm{d}\tau_0} (\cos x_0) \mathrm{d}\tau_0$$

with $\cos x_0 = -k_0 \,\mathrm{sn}(\tau_0 + \psi, k_0)$. Define I by

$$I = \frac{1}{T} \int_0^T \lambda(\tau_0) \frac{\mathrm{d}}{\mathrm{d}\tau_0} (\cos x_0) \mathrm{d}\tau_0$$

which is equivalently

$$I = -\frac{k_0}{T}\int_0^T \lambda(\tau_0)\,\mathrm{cn}\,(\tau_0+\psi)\,\mathrm{dn}\,(\tau_0+\psi)\,\mathrm{d}\tau_0.$$

The limits of the integration are over a period but are between points where $\mathrm{d}x_0/\mathrm{d}\tau_0 = 0$. These are where $\mathrm{dn}\,(\tau_0+\psi) = \pm K_0$ or $\mathrm{cn}\,(\tau_0+\psi) = 0$, so the limits are $T/4-\psi$ and $5T/4-\psi$. We now let $\tau_0+\psi = s$ to give

$$I = -\frac{k_0}{T}\int_{T/4}^{5T/4} \lambda(s-\psi)\,\mathrm{cn}\,(s)\,\mathrm{dn}\,(s)\,\mathrm{d}s.$$

If $\lambda = \lambda_0\cos^2\phi = \frac{1}{2}\lambda_0(1+\cos 2\phi)$, then

$$I = -\frac{k_0\lambda_0}{2T}\int_{T/4}^{5T/4} (1+\cos 2s\cos 2\psi - \sin 2s\sin 2\psi)\,\mathrm{cn}\,(s)\,\mathrm{dn}\,(s)\,\mathrm{d}s.$$

Evaluating the first integral we find

$$\int_{T/4}^{5T/4} \mathrm{cn}\,(s)\,\mathrm{dn}\,(s)\,\mathrm{d}s = \mathrm{sn}\,(s)\,|_{T/4}^{5T/4} = 0$$

since $\mathrm{sn}\,(T+x) = \mathrm{sn}\,(x)$. We now get

$$I = A\cos 2\psi + B\sin 2\psi,$$

$$A = -\frac{k_0\lambda_0}{2T}\int_{T/4}^{5T/4} \cos 2s\,\mathrm{cn}\,(s)\,\mathrm{dn}\,(s)\,\mathrm{d}s,$$

$$B = \frac{k_0\lambda_0}{2T}\int_{T/4}^{5T/4} \sin 2s\,\mathrm{cn}\,(s)\,\mathrm{dn}\,(s)\,\mathrm{d}s$$

so that

$$\frac{\mathrm{d}k_0^2}{\mathrm{d}\tau_1} = 4K_0^2(A\cos 2\psi + B\sin 2\psi).$$

By definition

$$\frac{\mathrm{d}\tau}{\mathrm{d}\phi} = 1-\epsilon\lambda(\phi)(1-2\cos x),$$

so to lowest order we identify τ_0 with ϕ and since $\tau \equiv \tau_0+\psi$,

$$\frac{\mathrm{d}\psi}{\mathrm{d}\phi} = -\frac{\epsilon}{T}\int_0^T \lambda(\phi)(1-2\cos x_0)\,\mathrm{d}\phi$$

where we have removed the periodic variation in $\dot{x}$ and, because of the ϵ preceding the integral, we can take the lowest-order value of x. With $\tau_0 \equiv \phi$, $\epsilon\phi \equiv \tau_1$ the above gives

$$\frac{\mathrm{d}\psi}{\mathrm{d}\tau_1} = \frac{1}{T}\int_0^T \lambda(\phi)(1-2\cos x_0)\,\mathrm{d}\phi$$

$$= -\lambda_0\left\{\frac{1}{2}+\frac{\sin 2T}{4T}\right\}+\frac{2\lambda_0}{T}\int_0^T \cos^2\phi\cos x_0\,\mathrm{d}\phi.$$

We note that

$$\frac{1}{T}\int_0^T \cos^2\phi\cos x_0\,\mathrm{d}\phi = -\frac{k_0}{T}\int_0^T \cos^2\tau_0\,\mathrm{sn}\,(\tau_0+\psi)\,\mathrm{d}\tau_0.$$

If we choose the limits of integration as before we get

$$\frac{1}{T}\int_0^T \cos^2\phi \cos x_0 \,\mathrm{d}\phi = -\frac{k_0}{T}\int_{T/4}^{5T/4} \cos^2(s-\psi)\,\mathrm{sn}\,(s)\,\mathrm{d}s$$

$$= -\frac{k_0}{2}[D + \bar{A}\cos 2\psi + \bar{B}\sin 2\psi],$$

where

$$D = \frac{1}{T}\int_{T/4}^{5T/4} \mathrm{sn}\,(s)\,\mathrm{d}s,$$

$$\bar{A} = \frac{1}{T}\int_{T/4}^{5T/4} \cos 2s\,\mathrm{sn}\,(s)\,\mathrm{d}s,$$

$$\bar{B} = \frac{1}{T}\int_{T/4}^{5T/4} \sin 2s\,\mathrm{sn}\,(s)\,\mathrm{d}s.$$

Thus we have

$$\left.\begin{aligned} \frac{\mathrm{d}k_0^2}{\mathrm{d}\tau_1} &= 4K_0^2(A\cos 2\psi + B\sin 2\psi), \\ \frac{\mathrm{d}\psi}{\mathrm{d}\tau_1} &= -\lambda_0\left[\frac{1}{2} + \frac{\sin 2T}{4T}\right] - \lambda_0 k_0[D + \bar{A}\cos 2\psi + \bar{B}\sin 2\psi], \end{aligned}\right\} \tag{B 3}$$

where A, B, $\bar{A}$, $\bar{B}$, D are all functions of K_0.

Finally we integrate these equations over one period and write

$$\int_0^{\epsilon T} \frac{\mathrm{d}k_0^2}{\mathrm{d}\tau_1}\mathrm{d}\tau_1 = (k_0^2)_{n+1} - (k_0^2)_n$$

where n denotes the value after n iterations of the Poincaré Section. We treat the right-hand side of the equations as constant over this time scale so we finally obtain a map of the form

$$(k_0^2)_{n+1} = (k_0^2)_n + 4K_0^2\epsilon T[A\cos 2\psi_n + B\sin 2\psi_n],$$

$$\psi_{n+1} = \psi_n - \epsilon T H_n,$$

where H_n is the right-hand side of (B 3) evaluated at $k = k_n$ and $\psi = \psi_n$. This is a symplectic map and is of the form of maps arising in other branches of physics, as discussed by Lichtenberg & Liebermann (1982).

This map has not been studied in detail but preliminary calculations show that $A \sim B \sim 0$ for $k_0^2 = 0.8$ which shows the existence of a fixed point of the map for this value of k_0. The lowest-order solution x_0 is periodic with period three for $k_0^2 \sim 0.8$ and thus the fixed point of the map can be associated with the period-three island chain found numerically and illustrated in figure 10(*b*).

For $\epsilon = 0$ we see that k_0^2 is constant independent of n and the phase portrait is then as shown in figure 10(*a*) with each closed curve corresponding to a different value of k_0. For $\epsilon > 0$ we expect the emergence of a period-three island chain centred about a value of $k_0^2 \sim 0.8$. By analogy with the well-known results obtained from studies of, for example, the Chirikov map we expect the onset of chaotic regions as ϵ is increased and the emergence of a fully chaotic solution for sufficiently large values of ϵ.

REFERENCES

ACHARYA, N., SEN, M. & CHANG, H.-C. 1992 *Intl J. Heat Mass Transfer* **35**, 2475–2489.

AREF, H. 1984 Stirring by chaotic advection. *J. Fluid Mech.* **143**, 1–21.

AREF, H. 1990 Chaotic advection of fluid particles. *Phil. Trans. R. Soc. Lond.* A **333**, 273–288.

ARNOL'D, V. 1965 Sur la topologie des ecoulements stationnaires des fluides parfaits. *C. R. Acad. Sci. Paris* **261**, 17–20.

ARROWSMITH, D. K. & PLACE, C. M. 1990 *Introduction to Dynamical Systems.* Cambridge University Press.

ARTER, W. 1983 Ergodic stream-lines in steady convection. *Phys. Lett* A **97**, 171–174.

BALLAL, B. Y. & RIVLIN, R. S. 1977 Flow of a Newtonian fluid between eccentric rotating cylinders: Inertial effects. *Arch. Rat. Mech. Anal.* **62**, 237–294.

CHIRIKOV, B. V. 1979 A universal unstability of many-dimensional oscillator systems. *Phys. Rep.* **52**, 265–379.

COLE, J. A. 1965 Experiments on Taylor vortices between eccentric rotating cylinders. *Proc. 2nd Aust. Conf. Hydr. Fluid Mech.*

COLE, J. A. 1976 Taylor-vortex instability and annulus length effects. *J. Fluid Mech.* **75**, 1–15.

DAI, R.-X., DONG, Q. SZERI, A. Z. 1992 Flow between eccentric rotating cylinders: bifurcation and stability. *Intl J. Engng Sci.* **30**, 1323–1340.

DIPRIMA, R. C. 1963 A note on the stability of flow in loading journal bearings. *Am. Soc. Lub. Engrs Trans.* **6**, 249–253.

DIPRIMA, R. C. & STUART, J. T. 1972*a* Flow between eccentric rotating cylinders. *J. Lub. Tech. Trans. ASME*: **F94**, 266–274.

DIPRIMA, R. C. & STUART, J. T. 1972*b* Non-local effects in the stability of flow between eccentric rotating cylinders. *J. Fluid Mech.* **54**, 393–415.

DIPRIMA, R. C. & STUART, J. T. 1975 The nonlinear calculation of Taylor-vortex flow between eccentric rotating cylinders. *J. Fluid Mech.* **67**, 85–111.

DOMBRE, T., FRISCH, U., GREENE, J. M., HÉNON, M., MEHR, A. & SOWARD, A. M. 1986 Chaotic streamlines in the ABC flows. *J. Fluid Mech.* **167**, 353–391.

EAGLES, P. M., STUART, J. T. & DIPRIMA, R. C. 1975 The effects of eccentricity on torque and load in Taylor-vortex flow. *J. Fluid Mech.* **87**, 209–231.

HÉNON, M. 1965 Sur la topologie des lignes de courant dans un cas particulier. *C. R. Acad. Sci. Paris* **262**, 312–314.

JONES, S. W., THOMAS, O. M. & AREF, H. 1989 Chaotic advection by laminar flow in a twisted pipe. *J. Fluid Mech.* **209**, 335–357.

KOSCHMIEDER, E. L. 1976 Taylor vortices between eccentric cylinders. *Phys. Fluids* **19**, 1–4.

KARASUDANI, T. 1987 Non-axis-symmetric Taylor vortex flow in eccentric rotating cylinders. *J. Phys. Soc. Japan* **56**, 855.

LICHTENBERG, A. J. & LIEBERMANN, M. A. 1982 *Regular and Stochastic Motion.* Springer.

MACKAY, R. S. 1994 Transport in 3d volume-preserving flows. *J. Nonlinear Sci.* **4**, 329–354.

MARCUS, P. S. 1981 Effects of truncation in modal representations of thermal convection. *J. Fluid Mech.* **103**, 241–255.

O'BRIEN, K. T., JONES, C. D. & MOBBS, F. R. 1974 Separation and cavitation in superlaminar flow between eccentric rotating cylinders. In *Leeds–Lyon symposium on Tribology*, pp. 69–72.

OIKAWA, M., KARASUDANI, T. & FUNAKOSHI, M. 1989*a* Stability of flow between eccentric cylinders with a wide gap. *J. Phys. Soc. Japan* **58**, 2209–2210.

OIKAWA, M., KARASUDANI, T. & FUNAKOSHI, M. 1989*b* Stability of flow between eccentric rotating cylinders. *J. Phys. Soc. Japan* **58**, 2355–2364.

OTTINO, J. M. 1989 *The Kinematics of Mixing; Stretching, Chaos and Transport.* Cambridge University Press.

OZOGAN, M. S. & MOBBS, F. R. 1980 Superlaminar flow between eccentric rotating cylinders at small clearance ratios. In *Energy Conservation Through Fluid Film Lubrication Technology: Frontiers in Research and Design* (ed. S. M. Rohde, D. F. Wilcock & H. S. Cheng). The American Society of Engineers.

PRANDTL, L. 1905 *Verhandlungen des III Internationalen Mathematiker–Kongresses (Heidelberg* 1904), *Leipzig*, pp. 484–491. (Also in Prandtl, L. 1961, *Gesammelte Abhandlungen*, vol. 2, pp. 575–584. Springer.)

RAFFAÏ, R. & LAURE, P. 1991 Effets de l'excentrement des cylindres sur les premières bifurcations du problème de Couette–Taylor. *C. R. Acad. Sci. Paris* **313**, 179–184.

ROWLANDS, G. 1990 *Nonlinear Phenomena in Science and Engineering*. Ellis Horwood.

SZERI, A. Z. & AL-SHARIF, A. 1993 Flow between finite, steadily rotating eccentric cylinders. Preprint.

VERSTEEGEN, P. L. & JANKOWSKI, D. F. 1969 Experiments on the stability of viscous flow between eccentric rotating cylinders. *Phys. Fluids* **12**, 1138–1143.

VOHR, J. A. 1968 An experimental study of Taylor vortices and turbulence in flow between eccentric rotating cylinders. *Trans. ASME: J. Lub. Tech.* F**90**, 285–296.

WEINSTEIN, M. 1977*a* Wavy vortices in the flow between two long eccentric rotating cylinders, I. Nonlinear theory. *Proc. R. Soc. Lond.* A **354**, 441–457.

WEINSTEIN, M. 1977*b* Wavy vortices in the flow between two long eccentric rotating cylinders, II. Linear theory. *Proc. R. Soc. Lond.* A, **354**, 459–489.

WOOD, W. W. 1957 The asymptotic expansions at large Reynolds numbers for steady motion between non-co-axial rotating cylinders. *J. Fluid Mech.* **3**, 159–175.

ZARTI, A. S. & MOBBS, F. R. 1980 Wavy Taylor vortex flow between eccentric rotating cylinders. In *Energy Conservation Through Fluid Film Lubrication Technology: Frontiers in Research and Design* (ed. S. M. Rohde, D. F. Wilcock & H. S. Cheng). The American Society of Engineers, New York.